Spine

SPINE Volume 36, Number 11, pp E720–E726

DIAGNOSTICS

Impact of the O-C2 Angle on the Oropharyngeal Space in Normal Patients

Masato Ota, MD,* Masashi Neo, MD, PhD,* Tomoki Aoyama, MD, PhD,† Tatsuro Ishizaki, MD, PhD,‡ Shunsuke Fujibayashi, MD, PhD,* Mitsuru Takemoto, MD, PhD,* Takeo Nakayama, MD, PhD,‡ and Takashi Nakamura, MD, PhD,*

Study Design. Radiographic analysis using normal patients.

Objective. To analyze the relationship between the cervical alignment and the oropharyngeal space.

Summary of Background Data. Few clinical studies stress the effect of the occipito-C2 (O-C2) alignment on the oropharyngeal space. A previous study showed dysphagia and/or dyspnea after occipitocervical fusion was caused by oropharyngeal stenosis resulting from O-C2 fixation in a flexed position. Other independent researchers showed that development or improvement of obstructive sleep apnea in rheumatoid arthritis patients was related to the O-C2 alignment. However, there are limited basic data demonstrating the relationship between the O-C2 alignment and the oropharyngeal space.

Methods. Plain lateral cervical radiographs in five tested positions—neutral, flexion, extension, protrusion, and retraction—of 40 asymptomatic volunteers were collected. The O-C2 angle, the C2–C6 angle, and the anterior–posterior distance of the narrowest oropharyngeal airway space (nPAS) were measured, and the changes in value from the neutral to the other four positions were calculated for each patient.

Results. According to the multiple regression analysis, there was an extremely strong linear correlation of the change in the O-C2 angle with the percentage change in the nPAS. Referring to the multiple regression analysis, a decrease of 10° in the O-C2 angle caused a 37% reduction in the nPAS in the neutral position. In contrast, no significant correlation was found between the change in the C2–C6 angle and the percentage change in the nPAS.

Conclusion. Our results show the impact of the O-C2 angle on the oropharyngeal space. This knowledge will be useful for the diagnosis and treatment of the upper cervical lesion combined with the upper airway stenosis, and for the determination of the optimal fixation angle in occipitocervical fusion.

Key words: cervical alignment, protrusion, retraction, airway space, occipitocervical fusion, dysphagia, pharyngeal space.

Spine 2011;36:E720–E726

Dysphagia and/or dyspnea after posterior occipitocervical (O-C) fusion have been recognized as a serious postoperative complication.[1,2] The exact cause is unknown, but it is empirically known that a posterior total cervical fusion from the occiput to the thoracic spine in a flexed position may bring about these complications.[2,3] Therefore, many surgeons believe that the total sagittal alignment of the cervical spine is important to avoid these complications. However, optimal or safe cervical alignment is not known because it is complicated. It includes protrusion and retraction positions, and flexion and extension positions, and the reduction of atlantoaxial or vertical subluxation during operation also changes the alignment.[4–6] Therefore, it is widely believed to be safe that total O-C fusion should be performed after confirming the comfortable position using a halo-vest fixation.[2]

Recently, however, two quite different clinical studies have stressed the impact of the occipito-C2 (O-C2) alignment on the oropharyngeal space. The authors reported that the change in the alignment of a very short segment, that is, only O-C2, does impact the postoperative dysphagia and/or dyspnea by reducing the cross-sectional area of the oropharynx.[7] This conclusion was strongly supported by independent research by Ataka et al.[8] They revealed that obstructive sleep apnea (OSA) in rheumatoid arthritis (RA) patients with an upper cervical spine lesion improved after O-C fusion when the O-C2 was fixed in a more extended position. Conversely, OSA did not improve when their O-C2 alignment changed minimally after surgery. These two clinical researches from different standpoints suggest that the oropharyngeal space is not closely related with total cervical spine alignment but with O-C2 alignment. If this is true, it should impact the diagnosis and treatment of the upper cervical spine lesion.

From the *Department of Orthopaedic Surgery, Graduate School of Medicine, Kyoto University, Japan; †Department of Human Health Sciences, Graduate School of Medicine, Kyoto University, Japan; and ‡Department of Health Informatics, Kyoto University School of Public Health, Japan.

Acknowledgment date: April 29, 2010. First Revision date: August 24, 2010. Accepted date: August 27, 2010.

The paper submitted does not contain information about medical device(s)/drug(s).

No funds were received in support of this work. No benefits in any form have been or will be received from a commercial party related directly or indirectly to the subject of this paper.

IRB Approval: The Institutional Review Board of Kyoto University Hospital approved the protocol of this study.

Address correspondence and reprint requests to Masashi Neo, MD, PhD, Department of Orthopaedic Surgery, Graduate School of Medicine, Kyoto University, 54 Kawahara-cho, Shogoin, Sakyo-ku, Kyoto 606-8507, Japan; E-mail: neo@kuhp.kyoto-u.ac.jp

DOI: 10.1097/BRS.0b013e3181f9f714

A few basic studies have investigated the relationship between the pharyngeal space and head posture, but the changes in the partial range of motion between cervical flexion and extension were merely examined.[9–11] Neck posture in the sagittal plane not only includes flexion and extension, but also protrusion and retraction. Protrusion consists of upper cervical extension and lower cervical flexion, and *vice versa* for retraction.[4–6,12,13] Therefore, assessment of these two positions, and flexion and extension, is essential to evaluate the impact of the O-C2 alignment on the oropharyngeal space.

In this study, we investigated the correlation of the O-C2 angle with the oropharyngeal space based on data obtained using plain cervical lateral radiographs at different cervical positions in normal patients. The purpose of this study was to show the major impact of the O-C2 alignment on the oropharyngeal space.

MATERIALS AND METHODS

Patient Population

Forty healthy volunteers, 20 males and 20 females, participated in this study. None of the patients had a history of neck pain, cervical surgery, respiratory disease, or temporomandibular joint disorders. The mean age of the patients was 38.2 ± 10.5 years (range 22–57 years), and the mean body mass index (BMI) was 21.3 ± 2.7 kg/m^2 (range 16.8–27.0 kg/m^2).

Written informed consent was obtained from all patients after the potential risks, and the aim of the study and procedures for imaging, were fully explained. The Institutional Review Board of our institute approved the protocol of this study.

Setup and Data Collection

Five plain lateral radiographs of the cervical spine were taken for each patient while in a sitting posture on an upright chair. The initial radiograph was taken in the neutral position for reference, and the next four radiographs were taken in the flexion (chin-to-chest), extension (face toward ceiling), protrusion (maximal forward gliding of the head), and retraction (maximal backward gliding of the head) positions (Figure 1). In an attempt to minimize upper thoracic motion, patients were instructed to maintain both their upper thoracic spine and shoulders in close contact with the back of the chair throughout the tests. As shown in Figure 1A, the neutral position was determined by the correspondence between the facial shadow, connecting the most anterior point of glabela with the mental protuberance, and the gravity line drawn on the surface of the film board. In the protrusion and retraction positions (Figure 1D, E), care was taken to attain the same conditions as the neutral position mentioned above to hold the patient's head at zero sagittal rotation. Photographs were also taken under the following conditions. Patients were instructed to maintain their shoulders as low as possible to facilitate radiography of the C6 vertebral body and not to swallow just before the radiograph was taken. A radiograph was taken at the end of tidal expiration with the centric occlusal position. The radiographic film cassette was 200 cm from the radiograph tube. The imaging center was focused on the external acoustic meatus and all nasion, external occipital protuberance, and cervicothoracic junctions were included in the radiograph. One radiologic technologist, who had been strictly educated to set proper cervical positions under our guidance, took all the radiographs.

RADIOGRAPHIC MEASUREMENTS

On 200 lateral radiographs of the cervical spine, the O-C2 angle, the C2–C6 angle, and the narrowest oropharyngeal airway space (nPAS) were traced and measured to evaluate the relation between cervical alignment and the oropharyngeal airway space. The O-C2 angle was defined as the angle between the McGregor's line and the line parallel to the inferior endplate of C2, and the C2–C6 angle was defined as

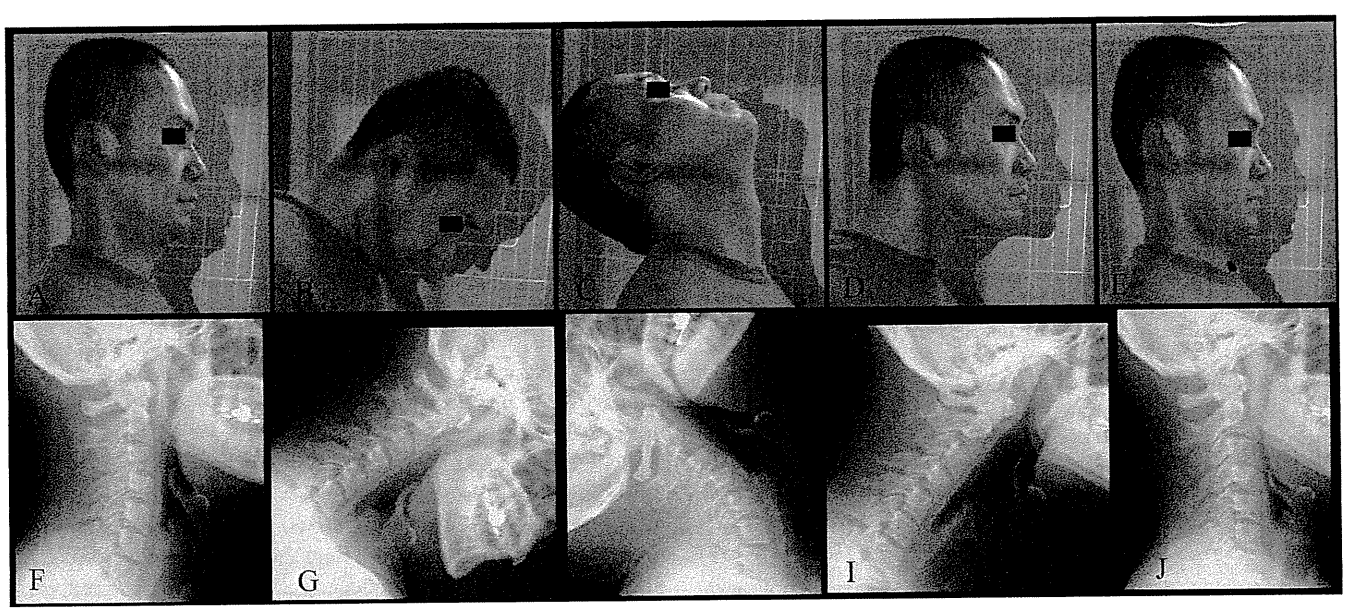

Figure 1. Five lateral cervical postures and radiographs in the neutral (**A**, **F**), flexion (**B**, **G**), extension (**C**, **H**), protrusion (**D**, **I**), and retraction (**E**, **J**) positions.

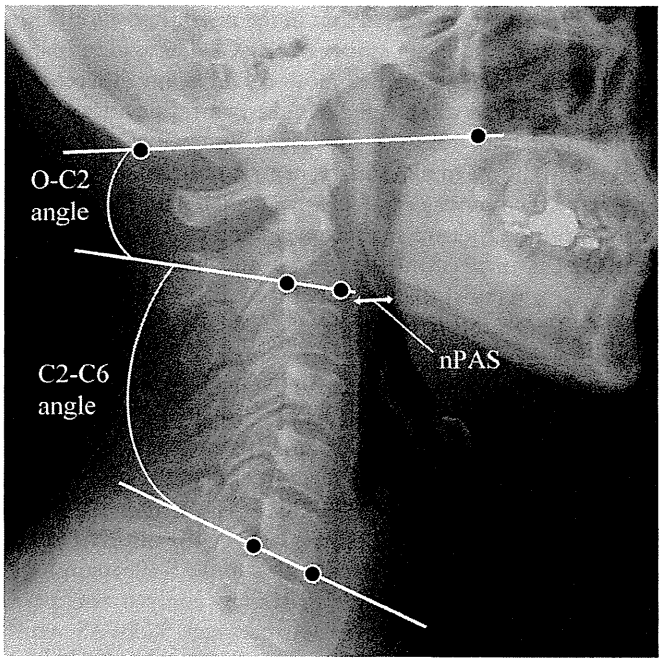

Figure 2. Representation of radiographic measurements. The O-C2 angle represents the angle between the McGregor's line and the inferior endplate of C2. The C2–C6 angle represents the angle between the inferior endplates of C2 and C6. nPAS represents the narrowest anterior–posterior distance from the posterior pharyngeal wall to the back of the tongue between the levels of the uvula tip and the epiglottis tip.

the angle between the lines parallel to the inferior endplate of C2 and C6 vertebral bodies (Figure 2). A positive value of both O-C2 and C2–C6 angles indicated a lordosis at the measured segments. The nPAS was obtained by measuring the shortest anterior–posterior distance from the posterior pharyngeal wall to the back of the tongue between the levels of the uvula tip and the epiglottis tip, as illustrated in Figure 2.

The first author traced and recorded all radiographic landmarks. To identify the landmarks accurately, the contrast and brightness of the images were regulated using a Centricity PACS system version 2.0 (GE healthcare, Milwaukee, WI). All linear and angular parameters were calculated with a precision of 0.1 mm and 0.1°, as dictated by this workstation. To ensure consistency, 100 randomly selected radiographs were traced and measured twice on another day. To evaluate the error of the method, the difference between the means of the first and second tracings for each of the variables was tested using paired *t* tests. No statistical significant difference was noted.

Evaluation of the Correlation of the O-C2 Angle or the C2–C6 Angle with the nPAS

To analyze the correlations of the O-C2 angle or the C2–C6 angle with the nPAS, the differences between the value in each of the four positions (X position), except the neutral position, and the value in the neutral position were calculated for each patient. The difference in the O-C2 angle (dOC2A) and C2–C6 angle (dC2C6A) were defined as dOC2A = O-C2 angle in X position – O-C2 angle in neutral position (degree) and dC2C6A = C2–C6 angle in X position − C2–C6 angle in neutral position (degree), respectively. To diminish the effect of the patient's body size on the pharyngeal space, the %dnPAS was employed as: %dnPAS = (nPAS in X position − nPAS in neutral position)/nPAS in neutral position × 100 (%).

STATISTICAL ANALYSIS

The means and standard deviations for the O-C2 angle, the C2–C6 angle, and the nPAS were calculated for each tested position. The values between the two positions were compared using the Tukey multiple comparison test. We used a multiple regression analysis to examine the association of %dnPAS with either dOC2A or dC2C6A, with %dnPAS as the dependent variable. The independent variables were age, sex, BMI, dOC2A, and dC2C6A. There were 160 analyzable data points from 40 patients, because each patient had a total of four data points to allow calculations for %dnPAS, dOC2A, and dC2C6A. In the regression model, we checked the assumptions of normality, linearity, homoscedasticity, and independence of the residuals. All reported *P* values are two-tailed, and the level of statistical significance was $P < 0.05$. We used SPSS software version 16.0 (SPSS Inc., Chicago, IL) for all analyses.

RESULTS

Table 1 lists the means and standard deviations for the O-C2 angle, the C2–C6 angle, and the nPAS for each tested

TABLE 1. Morphological Measurements

	Retraction (R) (n = 40)	Flexiontion (F) (n = 40)	Neutral (N) (n = 40)	Extension (E) (n = 40)	Protrusion (P) (n = 40)	Group difference* (P < 0.05)
O-C2 angle (°)	8.8 ± 6.5	11.6 ± 6.1	15.6 ± 6.7	35.1 ± 7.0	37.2 ± 8.4	E, P > N R < N
C2–C6 angle (°)	−6.3 ± 10.7	−24.7 ± 8.4	−2.1 ± 10.5	37.7 ± 9.8	1.1 ± 10.0	E > N F < N
nPAS (mm)	8.1 ± 3.5	10.6 ± 3.7	11.1 ± 3.2	18.4 ± 5.6	18.7 ± 5.4	E, P > N R < N

Note: Values are mean ± standard deviation.
**Tukey multiple comparison test.*
nPAS, the narrowest oropharyngeal airway space.

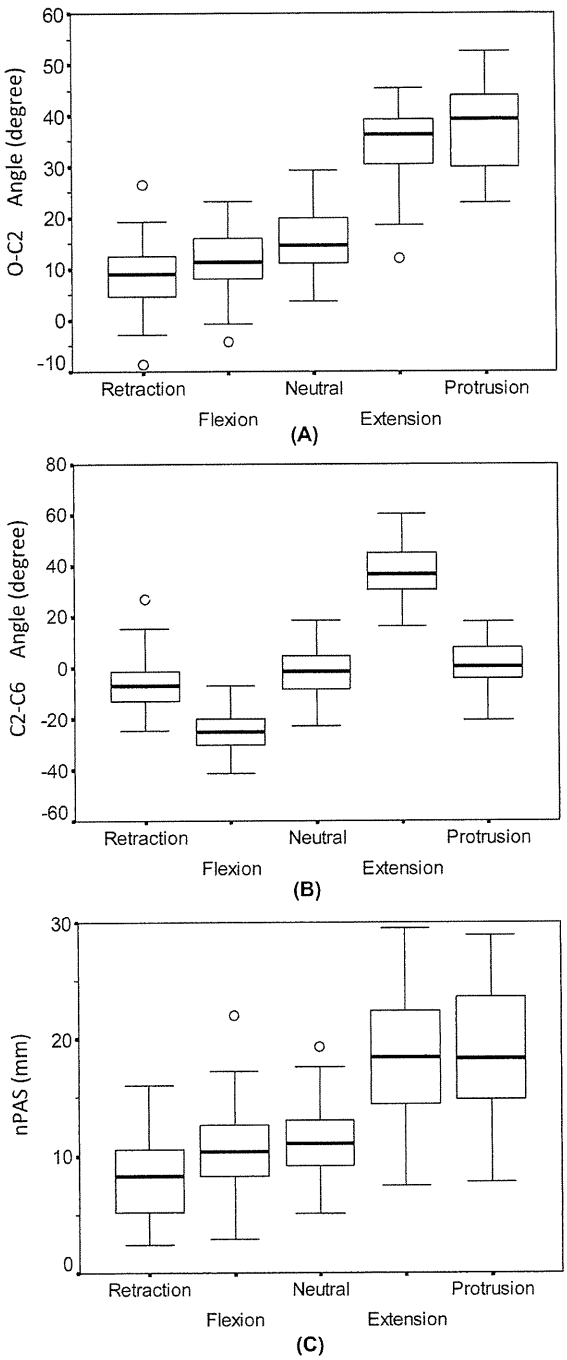

Figure 3. Box-and-whisker plots for each of the five tested positions. **A**, O-C2 angle; **B**, C2–C6 angle; **C**, nPAS. The patterns in A and C are the same but B is different. (nPAS represents the narrowest oropharyngeal airway space).

position. Figure 3 shows the box-and-whisker plots. The mean O-C2 angle in both extension and protrusion was significantly greater than that in the neutral position. The mean value in retraction was significantly smaller than in the neutral position, but no significant difference was found between the mean O-C2 angle in the flexion and neutral positions. The mean C2–C6 angle in extension was significantly greater than that in the neutral position, and the mean value in flexion was significantly smaller than that in the neutral position. On the other hand, the mean values of the C2–C6 angle in neither protrusion nor retraction showed significant differences compared with the C2–C6 angle in the neutral position. The mean nPAS in both extension and protrusion was significantly greater than the mean nPAS in the neutral position. The mean value in retraction was significantly smaller than that in the neutral position, but no significant difference was found between the mean nPAS in the flexion and neutral positions. Figure 3 clearly shows that the patterns of the box-and-whisker plots are almost the same for the O-C2 angle and the nPAS, but not for the C2–C6 angle.

Table 2 lists the mean values and standard deviations for dOC2A, dC2C6A, and %dnPAS. The scatter diagram between dOC2A and %dnPAS (Figure 4A) revealed that there was a strong positive linear correlation of dOC2A with %dnPAS (Pearson $r = 0.839$, $P < 0.001$). The scatter diagram between dC2C6A and %dnPAS (Figure 4B) showed that dC2C6A was weakly correlated with %dnPAS (Pearson $r = 0.392$, $P < 0.001$). A multiple regression analysis was performed to examine the association between %dnPAS with dOC2A, and dC2C6A (Table 3). The results identified that dOC2A was extremely correlated with %dnPAS [standardized regression coefficient (β) = 0.900, $P < 0.001$]. Conversely, no statistically significant correlation was found between dC2C6A and %dnPAS ($\beta = -0.082$, $P = 0.115$). The residual analyses revealed that the assumptions of normality, linearity, and homoscedasticity were not violated. Furthermore, 160 measurements obtained from 40 patients were analyzed using this multiple linear regression model and this might violate independence of the residuals in the model; however, the assumption of independence of the residuals was not violated (Durbin–Watson statistics = 1.96) in the model. The multiple regression equation was obtained as follows: %dnPAS = 3.71 × dOC2A − 0.20 × dC2C6A + 12.07 × WOMEN + 0.09 × AGE − 0.56 × BMI − 8.40 ($R^2 = 0.717$). This means that a decrease of 1° in dOC2A caused a reduction of 3.7% in the %dnPAS.

DISCUSSION

Oropharyngeal stenosis is speculated to be closely related to dysphagia and/or dyspnea after O-C fusion or OSA.[7,8,10,14,15] This study clearly shows that the occipito-upper-cervical alignment (O-C2 angle) has a great impact on the oropharyngeal space (nPAS), but that the middle-lower cervical alignment (C2–C6 angle) does not. It may be difficult to understand the significant relationship between the O-C2 angle and the nPAS intuitively because the occiput and C2 exist at a higher level than the oropharynx (Figure 2). This is probably the main reason why the close relationship between the O-C2 angle and the oropharyngeal stenosis has not been noticed by spinal surgeons thus far. Based on the previous reports,[7,8,14,16,17] we speculate that the mechanism of oropharyngeal stenosis caused by the reduction of the O-C2 angle is as follows. Soft tissue surrounds the oropharyngeal space, of which the anteriorly existing tongue root is the largest component. The soft tissue is then surrounded by a bony structure, the mandible

TABLE 2. Differences Between Each Position and the Neutral Position

	R–N	F–N	E–N	P–N
dOC2A (°)	−6.80 ± 3.53	−3.96 ± 4.57	19.5 ± 6.89	21.4 ± 8.90
dC2C6A (°)	−4.25 ± 7.76	−22.7 ± 7.91	39.8 ± 11.5	3.18 ± 10.5
%dnPAS (%)	−27.8 ± 20.2	−3.69 ± 26.0	68.2 ± 39.8	77.1 ± 58.0

Note: Values are mean ± standard deviation.

R, retraction; F, flexion; E, extension; P, protrusion; N, neutral; dOC2A = O-C2 angle in X position − O-C2 angle in neutral position; dC2C6A = C2–C6 angle in X position − C2–C6 angle in neutral position; %dnPAS = (nPAS in X position − nPAS in neutral position)/nPAS in neutral position × 100. (X position indicates flexion, extension, protrusion, or retraction position.)

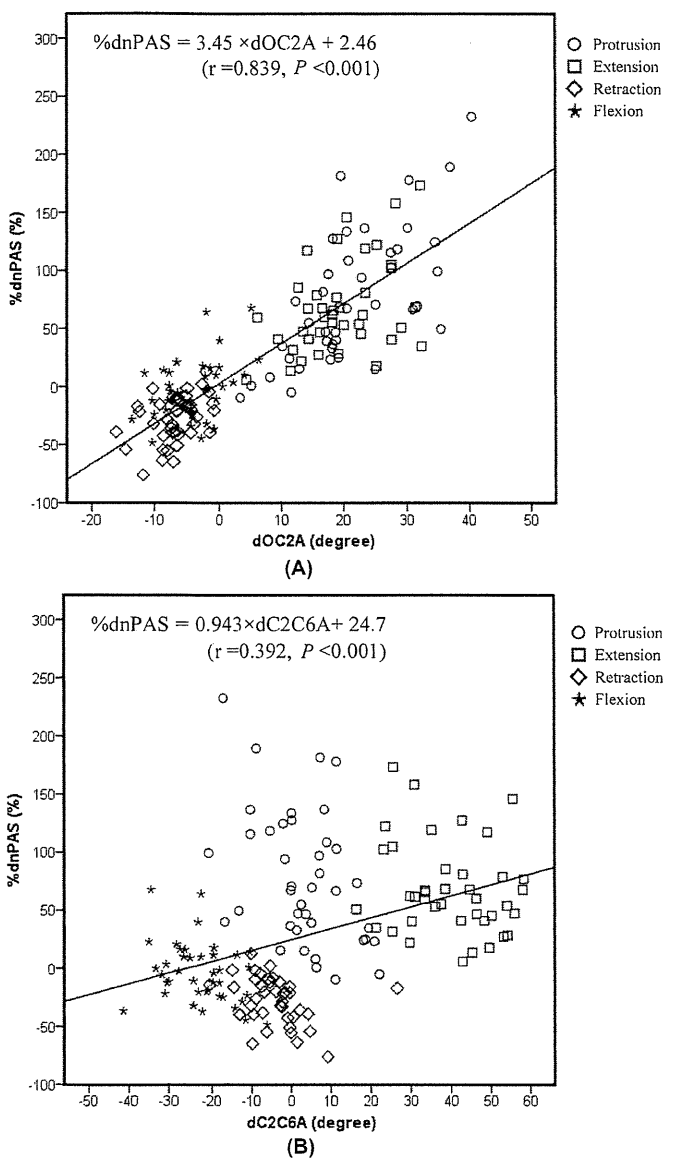

Figure 4. **A**, The scatter diagram between dOC2A and %dnPAS. **B**, The scatter diagram between dC2C6A and %dnPAS. dOC2A = O-C2 angle in X position − O-C2 angle in neutral position (degree); dC2C6A = C2–C6 angle in X position − C2–C6 angle in neutral position (degree); %dnPAS = (nPAS in X position − nPAS in neutral position)/nPAS in neutral position × 100 (%). (X position indicates flexion, extension, protrusion, or retraction position).

anteriorly and laterally, and the cervical spine posteriorly. The reduction of the O-C2 angle moves the maxilla in a flexed position, which makes the mandible shift posteriorly. This shift of the mandible reduces the volume of the bony container around the oropharyngeal level, resulting in an airway stenosis at this level. The authors previously found a downward displacement (posterior shift) of the tongue root in patients who developed a reduction in the O-C2 angle and subsequent dysphagia and/or dyspnea after O-C fusion.[7] This finding also supports the aforementioned mechanism.

Previous papers from different medical fields also support our conclusion. Muto et al, oral surgeons, investigated the relationship between the craniocervical inclination and the nPAS by measuring parameters at different degrees of cervical flexion and extension in the same patients.[10] They showed that the angle between the nasion-sella line (base line of the skull) and the tangent line of the posterior surface of C2 has close relationship to the nPAS. Their results are fairly consistent with this results, but our data are more convincing because we reached our conclusion by analyzing four different combinations of upper and lower cervical spine positions. Isono et al, anesthesiologists, endoscopically examined the cross-sectional area of the pharynx in completely anesthetized patients with OSA.[14] They clarified that protrusion was structurally beneficial to the maintenance of the pharyngeal airway because the change from the neutral to the protrusion position significantly enlarged it. Their results are also consistent with ours, because the O-C2 angle becomes larger in protrusion compared to the neutral position (Table 1 and Figure 3).

The O-C2 angle would be a very useful tool in spine surgery. It is well known that the major part of flexion and extension occurs at O-C1. We measured O-C2 angle, however, because it is much more popular to perform O-C2 fusion than O-C1 fusion, and O-C2 angle has been widely used as a landmark of O-C alignment.[1,7,8,18,19,20] In their previous study, the authors recommended that the O-C2 angle in O-C fusion should be kept at least at more than the preoperative O-C2 angle in the neutral position to prevent postoperative dysphagia and/or dyspnea.[7] Ataka et al showed that most of the OSA in RA patients with an upper cervical lesion is of an obstructive type because of a decreased O-C2 angle and subsequent oropharyngeal stenosis.[8] They also showed that O-C fusion with a more extended O-C2 position alleviates their symptoms. The measurement of the O-C2 alignment using the McGregor line and C2 endplate line has been proved to be

TABLE 3. Association of dOC2A or dC2C6A with %dnPAS from the Multiple Regression Analysis

		95% Confidence interval			
	B	Lower limit	Upper limit	β	*P*
dOC2A (°)	3.71	3.28	4.13	0.900	<0.001*
dC2C6A (°)	−0.197	−0.443	0.049	−0.082	0.115

All coefficients were adjusted for age, sex, and BMI.

R^2 = 0.717; B, unstandardized regression coefficient; β, standardized regression coefficient; dOC2A = O-C2 angle in X position − O-C2 angle in neutral position; dC2C6A = C2–C6 angle in X position − C2–C6 angle in neutral position; %dnPAS = (nPAS in X position − nPAS in neutral position)/nPAS in neutral position × 100. (X position indicates flexion, extension, protrusion, or retraction position.)

reproducible and is widely used.[7,8,18–20] The mean value of the O-C2 angle in the neutral position in this study was around 15°, which was consistent with previous reports.[18,19] However, its absolute value is variable between individuals,[19] and the change from the neutral position would be clinically more important. Therefore, we have no recommended O-C2 angle value. The greatest merit of the O-C2 angle is that it is easily measured using a C-arm during surgery. Usually it is difficult to determine the individual optimal cervical alignment macroscopically or radiographically in the prone position on the operating table. Although anatomic factors, such as obesity, micrognathia, and retrognathia, and dynamic factors, such as body positions and pharyngeal dilator muscle activities, also contribute to the development of dysphagia or OSA,[14,21–25] we believe that most of the deterioration after fusion surgery could be avoided by measuring the O-C2 angle and adjusting it before final fixation.

In this study, protrusion and retraction radiographs were used. Protrusion consists of upper cervical extension and lower cervical flexion, and *vice versa* for retraction. Ordway et al measured the motion of each vertebral segment in these positions,[4,5] and our results concerning the change of the O-C2 (upper cervical) and the C2–C6 (middle-lower cervical except C6/7) angles in each position are well consistent with their results. Spine surgeons should notice that these positions are quite different from flexion or extension when they perform O-C fusion. For example, it is risky for postoperative oropharyngeal stenosis to put a patient in the retraction position at O-C fusion to facilitate the access to the upper cervical region.

We also present quantitative data regarding the relationship between the O-C2 angle and the nPAS. The results from the multiple regression analysis indicate that a decrease in the O-C2 angle by 10° brings about a reduction of the oropharyngeal airway space in the neutral position of approximately 37%. Thus, a small change in O-C2 angle has a great impact on the oropharyngeal space, but it is very difficult to detect such a change macroscopically. This fact stresses the importance of the O-C2 angle measurement during surgery.

In conclusion, the authors showed that the O-C2 angle, among many factors, is a key to deciding the oropharyngeal space. This may be confirmed by further cadaver studies. The O-C2 angle is easily measured; therefore, it will be a simple and practical parameter in the diagnosis and treatment of the upper cervical lesion.

➢ Key Points

- ❑ Five lateral cervical radiographs taken in neutral, flexion, extension, protrusion, and retraction positions of 40 healthy volunteers were investigated as for cervical alignment and oropharyngeal space.
- ❑ The oropharyngeal space was not associated with C2–C6 alignment, but strongly correlated with O-C2 alignment.
- ❑ Based on the multiple regression analysis, a decrease in the O-C2 angle by 10° caused a reduction of the narrowest oropharyngeal airway space in the neutral position of approximately 37%.
- ❑ The O-C2 angle would be a simple and practical parameter in the diagnosis and treatment of the upper cervical lesion with the oropharyngeal stenosis, and for the determination of the optimal fixation angle in occipitocervical fusion.

Acknowledgments

The authors thank the following individuals for their helpful discussion in this study: Prof. Kazuo Chin, Department of Respiratory Care and Sleep Control Medicine, Graduate School of Medicine, Kyoto University, Kyoto, Japan; and Dr. Tomohiro Handa and Dr. Kensaku Aihara, Department of Respiratory Medicine, Graduate School of Medicine, Kyoto University, Kyoto, Japan. The authors are also grateful to the radiologic technologists who cooperated in taking radiographs, Mr. Ryuzou Tanaka, Mr. Kenichi Ogawa, Mrs. Sakiko Himeji, and Mr. Kohei Yamaoka.

References

1. Yoshida M, Neo M, Fujibayashi S, et al. Upper-airway obstruction after short posterior occipitocervical fusion in a flexed position. *Spine* 2007;32:E267–70.
2. Bagley CA, Witham TF, Pindrik JA, et al. Assuring optimal physiologic craniocervical alignment and avoidance of swallowing-related complications after occipitocervical fusion by preoperative halo vest placement. *J Spinal Disord Tech* 2009;22:170–76.
3. Matsuyama Y, Kawakami N, Yoshihara H, et al. Long-term results of occipitothoracic fusion surgery in RA patients with destruction of the cervical spine. *J Spinal Disord Tech* 2005;18(Supp 1):S101–6.
4. Ordway NR, Seymour R, Donelson RG, et al. Cervical sagittal range-of-motion analysis using three methods: Cervical range-of-motion device, 3space, and radiography. *Spine* 1997;22:501–8.

5. Ordway NR, Seymour RJ, Donelson RG, et al. Cervical flexion, extension, protrusion, and retraction: a radiographic segmental analysis. *Spine* 1999;24:240–7.
6. Maeda T, Saito T, Harimaya K, et al. Atlantoaxial instability in neck retraction and protrusion positions in patients with rheumatoid arthritis. *Spine* 2004;29:757–62.
7. Miyata M, Neo M, Fujibayashi S, et al. O-C2 angle as a predictor of dyspnea and/or dysphagia after occipitocervical fusion. *Spine* 2009;34:184–8.
8. Ataka H, Tanno T, Miyashita T, et al. Occipitocervical fusion has potential to improve sleep apnea in patients with rheumatoid arthritis and upper cervical lesions. *Spine* 2010;35:E971–5.
9. Hellsing E. Changes in the pharyngeal airway in relation to extension of the head. *Eur J Orthodontics* 1989;11:359–65.
10. Muto T, Takeda S, Kanazawa M, et al. The effect of head posture on the pharyngeal airway space (PAS). *Int J Oral Maxillofac Surg* 2002;31:579–83.
11. Anegawa E, Tsuyama H, Kusukawa J, et al. Lateral cephalometric analysis of the pharyngeal airway space affected by head posture. *Int J Oral Maxillofac Surg* 2008;37:805–9.
12. Penning L. Normal movements of the cervical spine. *AJR Am J Roentgenol* 1978;130:317–26.
13. Penning L. Acceleration injury of the cervical spine by hypertranslation of the head: Part I. Effect of normal translation of the head on cervical spine motion: a radiological study. *Eur Spine J* 1992;1:7–12.
14. Isono S, Tanaka A, Ishikawa T, et al. Sniffing position improves pharyngeal airway patency in anesthetized patients with obstructive sleep apnea. *Anesthesiology* 2005;103:489–94.
15. Verbraecken JA, Backer WA. Upper airway mechanics. *Respiration* 2009;78:121–33.
16. Kuna ST, Remmers JE. Anatomy and physiology of upper airway obstruction. In:Kryger MH, Roth T, Dement WC eds. *Principles and Practice of Sleep Medicine*. 3 ed. Philadelphia: WB Saunders, 2000:840–58.
17. Inoko Y, Morita O. Influence of oral appliances on craniocervical posture in obstructive sleep apnea-hypopnea syndrome patients. *J Prosthodontic Res* 2009;53:107–10.
18. Matsunaga S, Onishi T, Sakou T. Significance of occipitoaxial angle in subaxial lesion after occipitocervical fusion. *Spine* 2001;26:161–5.
19. Shoda N, Takeshita K, Seichi A, et al. Measurement of occipitocervical angle. *Spine* 2004;29:E204–8.
20. Logroscino CA, Genitiempo M. Relevance of the cranioaxial angle in the occipitocervical stabilization using an original construct: a retrospective study on 50 patients. *Eur Spine J* 2009;18(Supp 1):S7–12.
21. Isono S, Tanaka A, Tagaito Y, et al. Influences of head positions and bite opening on collapsibility of the passive pharynx. *J Appl Physiol* 2004;97:339–46.
22. Tsuiki S, Almeida FR, Bhalla PS, et al. Supine-dependent changes in upper airway size in awake obstructive sleep apnea patients. *Sleep Breathing* 2003;7:43–50.
23. Ono T, Otsuka R, Kuroda T, et al. Effects of head and body position on two- and three-dimensional configurations of the upper airway. *J Dent Res* 2000;79:1879–84.
24. Zhang W, Masumi S, Makihara E, et al. Effects of jaw, head and body positions on upper airway dimensions and maximum forced inspiratory airflow. *J Kyushu Dent Soc* 2009;63:8–17.
25. Soga T, Nakata S, Yasuma F, et al. Upper airway morphology in patients with obstructive sleep apnea syndrome: effects of lateral positioning. *Auris Nasus Larynx* 2009;36:305–9.

The American Journal of Pathology, Vol. 178, No. 3, March 2011

DOI: 10.1016/j.ajpath.2010.12.012

Tumorigenesis and Neoplastic Progression

Murine Leukemia Retrovirus Integration Induces the Formation of Transcription Factor Complexes on Palindromic Sequences in the Signal Transducer and Activator of Transcription Factor 5a Gene During the Development of Pre–B Lymphomagenesis

Tatsuaki Tsuruyama,* Takuya Hiratsuka,† Guang Jin,‡ Yukiko Imai,* Haruya Takeuchi,* Yasuhiro Maruyama,§ Kazuya Kanaya,§ Munetaka Ozeki,* Tetsuya Takakuwa,‡§ Hironori Haga,¶ Keiji Tamaki,* and Takuro Nakamura‡

From the Departments of Forensic Medicine and Molecular Pathology and Human Health Science,§ Graduate School of Medicine, Kyoto University, Kyoto; the Laboratory of Pathology,† Noe-saiseikai Hospital, Osaka; the Laboratory of Carcinogenesis Cancer Institute,‡ Tokyo; and the Department of Diagnostic Pathology,¶ Kyoto University Hospital, Kyoto, Japan*

Murine leukemia retrovirus (MLV) vectors are highly effective tools for introducing a foreign gene into a target host genome. However, it remains unclear how integrated retroviral promoter activity is influenced by the upstream or downstream sequences and how the host cell phenotype is influenced by the integrated promoter activity. Herein, we analyzed a set of pre–B lymphoma clones in which the *MLV* genome was integrated into the signal transducer and activator of transcription factor 5a (*Stat5a*) gene. Among the clones, the lymphoma clones with a provirus integrating into the middle position of the palindromic target sequences showed significantly higher transcription of the *Stat5a* gene; and p300 and other transcriptional factors formed complexes, with binding to the proviral-host junctional DNA segment. By using a luciferase assay, the upstream and downstream sequences of the provirus contributed to the up-regulation of proviral promoter activity. In concomitance with the higher *Stat5a* transcription, the immunoglobulin gene recombination was arrested. Antiapoptotic activity was significantly higher, with an increase in Bcl-xL, one of the targets of STAT5A, when IL-7 was supplied. Thus, a minute difference between MLV integration sites can lead to large differences in the host phenotype through the formation of transcription factor complexes on the proviral-host junctional DNA segment, suggesting that caution is necessary in monitoring integration sites when working with MLV vectors. *(Am J Pathol 2011, 178:1374–1386; DOI: 10.1016/j.ajpath.2010.12.012)*

Retrovirus-based vectors have been used as an available tool for the introduction of a gene into the host genome in gene function analyses. Transgene transcription is predominantly controlled by the integrated retroviral promoter element in the long terminal repeat (LTR) in the vector sequence. However, because the retroviral promoter activity is affected by the integration site, the expression of a transgene is not necessarily adequate. The lack of control of retroviral integration limits its application in transgenic animal studies and gene therapy, which first and foremost must be safe for patients. Indeed, there is some risk that a murine leukemia retrovirus (MLV)–based vector could induce host malignant transformation by integration into an oncogene in the genome of a patient undergoing gene therapy.[1] Therefore, considerable attention has been given to the choice of appropriate vector integration sites for the induction of induced pluripotent stem cells from mouse embryonic or adult fibroblasts.[2] In fact, lack of control over

Supported by a Grant-in-Aid for Cancer Research from the Ministry of Education, Culture, Sports, Science and Technology of Japan and by the Ministry of Health, Labor and Welfare of Japan (grant 7013086 to T.N. and T.T.).

K.T. and T.N. contributed equally to this work.

Accepted for publication December 1, 2010.

None of the authors disclosed any relevant financial relationships.

Supplemental material for this article can be found at *http://ajp.amjpathol.org* or at doi:10.1016/j.ajpath.2010.12.012.

Address reprint requests to Tatsuaki Tsuruyama, M.D., Ph.D., Department of Forensic Medicine and Molecular Pathology, Graduate School of Medicine, Kyoto University, Yoshidakonoecho, Sakyo-ku, Kyoto 606-8501, Japan. E-mail: tsuruyam@fp.med-u.ac.jp or tsuruyam@kuhp.kyoto-u.ac.jp.

the integration site has limited the application of MLV vectors; it remains unclear to what extent the integration site influences retroviral promoter activity and host phenotype changes.

Furthermore, proviral promoter activity was compared under the expression of diverse—and not common—genes, which makes it impossible to render a consistent comparison. Because of these limitations associated with previous studies, the factors contributing to making proviral promoter activity exceedingly sensitive to minute nucleotide differences in the integration sites remain largely unstudied. The present investigation used comparative analysis of the activity of the MLV promoter integrated into an identical intron of the signal transducer and activator of transcription factor 5a (*Stat5a*) gene. We report that the activity is significantly influenced by the sequences flanking the retroviral integration sites and that the expression levels of the host gene can alter the host cell phenotype, as exemplified by hematopoietic cell differentiation and tumorigenesis induced by MLV integration.

In this article, we used a set of pro– to pre–B lymphoma clones containing the *MLV* genome integrated into variable sites within the second intron of the *Stat5a* gene, which is one of the common integration sites of MLV.[3,4] The encoded protein is a member of the STAT family and forms a dimer that translocates into the nucleus and exerts transcriptional activity by binding to the gamma interferon activation site element in the promoter of target antiapoptotic genes, such as *c-myc*, *pim-1*, *bclxL*, and cyclin D1,[5] that regulate proliferation and antiapoptosis in hematopoietic cells.[6,7] This signaling molecule in the IL-7 receptor pathway is limitedly operative during the precursor stage in the pro– to pre–B-cell lineage.[8] The STAT5A contributes to IL-7–induced B-cell precursor expansion.[9] Schwaller et al[10] have reported that *Stat5a* is essential for the myeloproliferative and lymphoproliferative diseases induced by Janus kinases. We supported their evidence by identifying the pro– or early pre–B-cell lymphomas using MLV integration into *Stat5a*.[4]

In the clones with MLV integration into *Stat5a*, we analyzed the correlation of the expression levels of the gene and MLV integration because varied STAT5A expression levels were expected to influence the degree of precursor expansion, probably affect Ig heavy chain (*IgH*) gene recombination in the host pre–B cells, and induce maturation arrest. To confirm the data on the MLV integration site and the expression levels of the target neighboring gene, we generated reporter gene assay vectors that consisted of the *MLV* genome either lacking or containing defective transcription factor–binding motifs within the retroviral LTR and the upstream and downstream sequences that originated from the *Stat5a* sequence. The downstream sequences were inserted upstream of luciferase as the reporter gene. Analysis of luciferase activity allowed us to investigate how different integration sites in the flanking sequence affect *MLV* promoter activity. Taken together, the data are consistent with the model presented herein for the control of retroviral promoter activity via interaction between the retroviral genome element and the host flanking sequence. The obtained data were used to construct a model demonstrating how a proviral genome in the target *Stat5a* sequence influences the proviral promoter activity and host cell phenotype.

Materials and Methods

Mice and Lymphoma Clones

All mice used in this study were handled in strict accordance with the guidelines for good animal practice, as defined by the relevant national and local animal welfare bodies; and all animal work was preapproved by the Kyoto University Ethics Committee for Animal Experiments. The SL/Kh mice were obtained from the RIKEN Bioresource Center, Tokyo, Japan. This strain possesses a pathogenetic endogenous ecotropic murine virus (*Emv11*) that was mapped on chromosome 7,[11] which is shared with the AKR/J mouse strain.[12] In addition, more than five copies of the endogenous murine leukemia retroviral genome, in addition to *Emv11*, are observed (Figure 1B, left). The identified endogenous MLV genomes are shown in Supplemental Table S1 (at *http://ajp.amjpathol.org*).

In the SL/Kh strain, the pro– to pre–B cells in the bone marrow (BM) acquire more than one copy of the proviral genome; and more than 90% of these mice develop BP-1$^+$ sIgM$^-$ pro– or pre–B lymphomas spontaneously by the age of 6 months.[4,11] Lymphoma cells of the swelling lymph node, 2.0×10^8, were obtained from a lymph node of a 6-week-old SL/Kh mouse and incubated in methylcellulose-based medium (Methocult) containing IL-7 for pro– to pre–B cells (Stemcell Technology, Vancouver, British Columbia, Canada) or in RPMI 1640 medium (Invitrogen, Carlsbad, CA) with 20-ng/ml IL-7, IL-3, IL-4, or stem cell factor (Peprotec, London, England).[4]

Southern Hybridization to Detect MLV Insertional Recombination in Stat5a

High-molecular-weight DNA samples were extracted from lymphoma and normal kidney tissues, and 2.5-mg aliquots of the DNA were digested with the NcoI restriction enzyme (New England Biolabs, Beverly, MA) for 16 hours and transferred to an N$^+$ nylon membrane (Hybond; GE Health Care, Buckinghamshire, England) after electrophoresis. The probe used was previously described.[4]

Inverse PCR Method for the Detection of the MLV Integration Site

The inverse PCR method was previously described.[4] The primers for inverse PCR were located within the *MLV* (EmvII) genomes. Their sequences were as follows: 5B4, 5′-GAGGGCTTGGACCTCTCGTCTCCTAAAAAACCACG-3′; and 5F1, 5′-GTCTCTCCCAAACTCTCCCCCTCTCCAACC-3′ (first set). In addition, these sequences were used: 5F2, 5′-CCTCCTCTGACGGAGATGGCGACAGAGAAGAGG-3′; and 5B1, 5′-GAGGGCTTGGACCTCTCGTCTCCTAAAAGAACCACG-3′ (second step of the cycles for nested PCR). The amplicons were then subcloned into a vector (pCR 2.1-TOPO; Invitrogen), and sequence analysis reactions were performed.

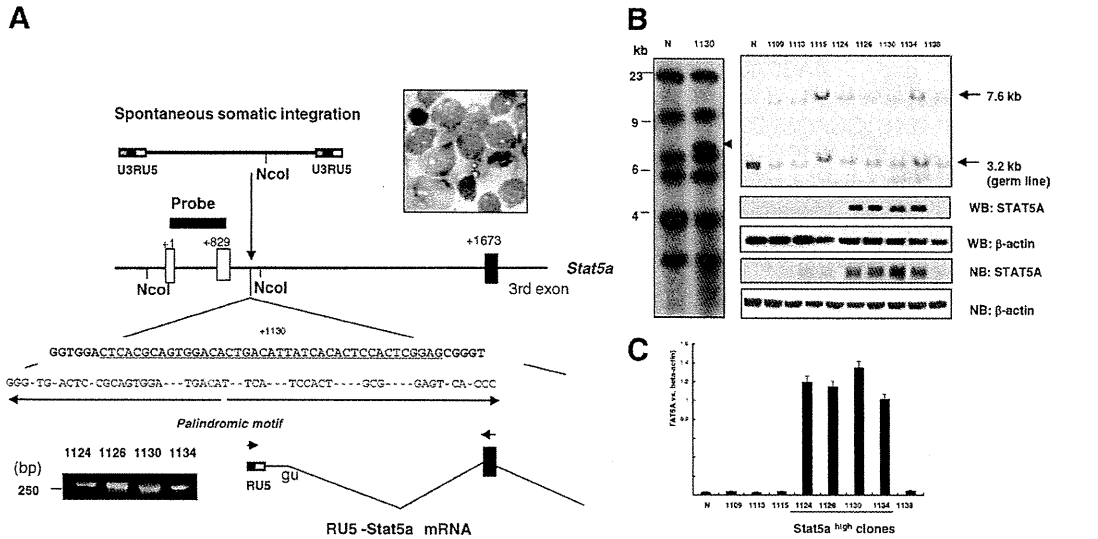

Figure 1. Genome integration of MLV provirus into *Stat5a*. **A:** Clones with MLV integration into the second intron of *Stat5a* (GENEBANK, AF049104). The two open boxes and the closed box in the *Stat5a* structure represent the untranslational exons and the third translational exon, respectively. The numbers represent the nucleotide number from the start of the gene. The detailed sequence of the integration site is shown. The underlining represents the flanking sequence used in the **i** through **vi** vector constructs in Figure 2A. The red letter in the sequence represents the position of integration site 1130 within the intron. Palindromic sequence motifs are shown at the bottom. NcoI sites are shown. The upper **inset** shows blastic lymphoma tissue from SL/Kh mice (Giemsa staining, original magnification ×600). Probe indicates the position of the probe used in the Southern hybridization assay.[4] The MLV-*Stat5a* chimera mRNA is shown below. The represented *gu* motif is the splicing signal sequence at the 1158 nucleotide. The bottom shows the result of the RT-PCR assay for chimera cDNA, including MLV RU5 (69 bp), the second intron (24 to 34 bp), and the third exon (158 bp) of *Stat5a*. Lane numbers represent the integration sites. **Arrows** represent the PCR primer positions. **B:** Southern blot of an NcoI-digested DNA fragment displaying the insertional recombination. **Left:** Six copies of an endogenous retroviral genome (N, 1130) and a newly acquired proviral genome (1130, **arrowhead**). **Right:** *Stat5a*-derived fragments are visualized. The upper **arrow** highlights the NcoI-digested fragment obtained after *Emv11* integration. Lane numbers represent the integration site. N indicates control BM pre–B cells of SL/Kh mice 3 weeks after birth; WB:STAT5A, Western blot of the lymphoma extract with an antibody for STAT5A. Fragments of 7.6 kb represent the NcoI-digested fragment obtained after MLV clonal integration. (β-Actin was the control blot.) NB:STAT5A is the Northern blot of lymphoma mRNA. (β-Actin was the control blot.) **C:** Relative intensity of STAT5A versus β-actin (control). The horizontal axis represents the nucleotide number from the start of the first exon of the *Stat5a* gene.

PCR for the Detection of Recombination in IgH and Ig Light Chain

The monoclonality was confirmed by PCR analysis after IgH diverse segment (D_H)–IgH J segment (J_H) recombination using primers designed to amplify four possible junctions between the D-Q52 and J_H regions. The primers were as follows: 5′-CACAGAGAATTCTCCATAGTTGATAGCTCAG-3′ (D_HQ52-1 [sense]) and 5′-AGGCTCTGAGATCCCTAGACAG-3′ (J_H4-1 [antisense]). The PCR conditions were as follows: denaturation for 1 minute at 95°C, annealing for 1 minute at 60°C, and extension for 2.5 minutes at 72°C (28 cycles). After D_H-Q52–J_H recombination, the monoclonal lymphoma cells were selected from the other cells and used for the following assays. For the analysis of V-J rearrangement, the degenerate V primer and another primer were used to amplify Vκ to J1-5κ rearrangement, as previously described.[13]

Flow Cytometry

A suspension of single cells was prepared from lymphoma tissue. The cells were adjusted to 10^6 cells/ml; the total lymphoma cell yield was in the range of 0.8×10^7 to 1.2×10^7 cells. A single-cell suspension was prepared from both SL/Kh and BALB/c mouse femur BM plugs, and their densities were adjusted to 10^6 cells/ml. The following antibodies were purchased commercially (BD Pharmingen, San Diego, CA): fluorescein isothiocyanate–labeled anti-BP1 (clone 6C3) and phosphatidylethanolamine-labeled anti-B220 (clone RA3-6B2). The collected cells were incubated with normal rat serum for 15 minutes and stained with 1:10,000 diluted monoclonal antibodies for 15 minutes. After washing, the cells were analyzed using a scanner (FACScan; Becton Dickinson, Mountain View, CA). The $BP1^+B220^+$ BM cells were purified from double-stained BM cells by cell sorting using a commercially available system (FACS Vantage; Becton Dickinson). The average yields from the BM cells of 4-week-old BALB/c and SL/Kh mice were 0.50% and 2.8%, respectively. Genomic DNA was extracted from the purified cells using a kit (QIAamp DNA Blood Mini Kit; QIAGEN GmbH, Hilden, Germany). Apoptotic lymphoma cells, 0.8×10^7 to 1.2×10^7, were stained using 5 ml of phosphatidylethanolamine-conjugated antibody (annexin V) at room temperature in the dark for 15 minutes. A 400-ml binding buffer was added for flow cytometry analysis.

Northern Blotting and RT-PCR Assay

The methods were previously described.[4] The RT-PCR was performed using extracted RNA with a one-step RT kit (Invitrogen). The primers used were as follows: actin, 5′-CCTAAGGCCAACCGTGAAAAG-3′ and 5′-TCTTCATGGTGCTAGGAGCCA-3′; terminal deoxytransferase, 5′-GAAGATGGGAACAACTCGAAGAG-3′ and 5′-CAGGTGCTGGAACATTCTGGGAG-3′; *Vpreb*, 5′-CGTCTGTCCTGCTCATGCT-3′ and 5′-ACGGCACAGTAATACACAGCC-3′;

CD79a, 5′-ATCACATGGTGGTTCAGCC-3′ and 5′-TCTCCAATGTGGAGGTTGC-3′; and *CD19*, 5′-TGTCTCTTCTGAGAAGCTGGC-3′ and 5′-AACCAGAAGTGGACCTGTGG-3′. The RT-PCR primers for the Ig κ light chain were as follows: 5′-GGCTGCAGSTCCAGTGGCAGTGGRTCWGGRAC-3′ and 5′-CATTCCTGTTGAAGCTCTTGACAATGGGTG-3′. The RT-PCR primers for the Ig λ light chain were as follows: forward, 5′-GCCTTTCTACACTGCAGTGGGTATGCAACAAT-3′; and reverse, 5′-AGCCACTYACCTAGGACAGTSASYTTGGTTCC-3′. For real-time PCR assays for the detection of proviral RNA in the lymphomas, total RNA was reverse transcribed using a kit (Omniscript RT kit; Qiagen). For relative quantification by RT-PCR, 20 ng of each cDNA was analyzed using a kit (FastStart DNA Master SYBR Green I; Roche Diagnostics, Mannheim, Germany) with software version 3.5. For each primer pair, a standard curve was developed. To detect *Emv11-Stat5a* chimera RNA, the following primer set was used: MLV U5–*Stat5a* exon3-1F, 5′-GAATCGTGGTCTCGCTGATC-3′; and MLV U5–*Stat5a* exon 3-1R, 5′-CCTGGAGCTGTGTGGCATAG-3′.

Antibodies for Western Blotting of STAT5A

Cell lysate was precleared using protein G–Sepharose (Sigma-Aldrich, St Louis, MO) at 4°C with 1 hour of agitation. The cleared lysate, 400 μL, was incubated with minimal essential medium 59, 50 μL, at 4°C overnight; then, protein G–Sepharose, 50 μL, was added and incubated for an additional hour. After centrifugation, immunocomplexes were washed three times with a radioimmunoprecipitation assay buffer (25 mmol/L Tris-HCl, pH 8.0; 150 mmol/L NaCl; and 1% NP40, a protease inhibitor mixture [Complete Mini EDTA-free; Roche Diagnostics]), resuspended in the sample buffer, and boiled for 5 minutes. The released proteins were examined by Western blotting. Antityrosine phosphorylated STAT5A was purchased from New England BioLabs (Ipswich, MA) and Santa Cruz Biotechnology (Santa Cruz, CA) (sc-11761). Purified anti-STAT5A and anti-STAT5B were obtained from ZYMED (San Francisco, CA). Antibodies toward β-actin (C4), p300 (sc-81349), GATA1 (sc-266), GATA2 (sc-267), Runx1 (sc-28679), Bcl-xL (sc-7122), CREB (sc-20), and CRE-BP1 (sc-8398) were also purchased from Santa Cruz Biotechnology (sc-47778). Streptavidin-peroxidase conjugate was acquired from DAKO (Gostrup, Denmark). The blot was measured using a chemiluminator (Aishin, Nagoya, Japan).

Vector Construction and Dual Luciferase Assay

For a reporter gene assay, Ba/F3 cells were obtained from RIKEN cell bank (Tsukuba, Japan). After a 12-hour recovery period in the 10-ng/ml IL-3–containing medium, the cells were incubated in an RPMI 1640 medium supplemented with 0.5% bovine serum albumin for 12 hours or stimulated with the cytokine for the last 6 hours. The Ba/F3 cells, 6.0×10^7, were transiently transfected by electroporation with 5 μg of a luciferase reporter plasmid. Electroporation was performed according to a previously reported protocol.[14] In each experiment, samples were analyzed in triplicate; and each experiment was repeated five times. On the other hand, lymphoma cells with the provirus integrating into *Stat5a* were maintained in an RPMI 1640 medium supplemented with 20% fetal calf serum, mercaptoethanol, and 50-mg/ml penicillin-streptomycin. Reporter gene analysis was performed 48 hours after transfection (Tecan, Durham, NC).

Cell lysate was then subjected to an assay (Dual-Luciferase Reporter Assay System; Promega, Madison, WI); a pGL3-basic vector lacking SV40 promoter (Promega) was used as the backbone for *Emv11*-derived provirus-firefly luciferase vectors (o, i, ii, iii, iv, v, vi, and vii) in the current study. The HindIII site (+53) in the multicloning site of the pGL3-basic vector was used to construct the firefly luciferase vector, including the *Emv11* proviral genome that was inserted into the identical orientation of the firefly luciferase and the flanking *Stat5a* sequence shown in the o through vii constructs for the assay. The flanking *Stat5a* sequence originated from the second intron. As a control for luciferase measurements in transfections, pRL-TK (HSV-tymidine tyrosine kinase) renilla luciferase (Promega) was cotransfected with a firefly luciferase vector. Firefly luciferase activity was normalized to renilla luciferase activity.

Preparation of MLV Integrase and Anti-Integrase

Full-length murine retroviral integrase cDNA (GENEBANK, J01998) was obtained from an SL/Kh mouse and subcloned into multiple cloning sites (EcoRI and XhoI) of the transfer vector (pSYNGCH; Katakura Industries, Saitama, Japan). The procedures for the construction of the recombinant virus and viral infection of silkworm *Bombyx mori* larvae have been reported.[15] To construct the recombinant baculovirus, Abv baculovirus DNA, a linearized AcNPV-BmNPV hybrid-type baculovirus DNA (Katakura, Maebashi, Japan), 0.5 mg, and psYNGCH-Th integrase, 1 mg, were used to cotransfect a monolayer of BmN cells, 2×10^6 cells/ml, in the presence of liposomes (Insectin; Invitrogen). These cotransfected BmN cells were maintained at 27°C in a culture for 5 days. Silkworm pupae were infected with the supernatants and harvested after 6 days. The pupae were homogenated by suspension in 30 ml of ice-cold homogenizing buffer A (20 mmol/L Tris-HCl, 150 mmol/L NaCl, 1 mmol/L EDTA, 1 mmol/L EGTA, 1 mmol/L dithiothreitol [DTT], and 0.05% phenylthiourea, pH 8.0) containing a protease inhibitor mixture (1 mmol/L phenylmethanesulfonyl fluoride and 10 mmol/L benzamidine) and disrupted at 3000 rpm for 5 minutes. The homogenate was centrifuged at 38,000 rpm for 1 hour at 4°C. After removal of the supernatant, the pellet was suspended in 30 ml of homogenizing buffer B (20 mmol/L Tris-HCl, 150 mmol/L NaCl, 1 mmol/L EDTA, 1 mmol/L EGTA, 1 mmol/L DTT, and 0.05% phenylthiourea, pH 8.0) containing the protease inhibitor mixture and thoroughly mixed in a homogenizer (Dounce Teflon) on ice at 1000 rpm for 10 strokes. The EDTA and DTT were added to the pellet at a final concentration of 10 mmol/L, followed by solubilization with a sulfobetaine detergent (Zwittergent 3-12; Calbiochem, San Diego). The

final concentration of the detergent was 2% w/v. The sample was stirred gently for 1 hour at 4°C and then centrifuged (Hitachi RP50-2 rotor) at 38,000 rpm for 1 hour at 4°C. The supernatant was collected, and the integrase was purified by column chromatography using the His-tag expressed on the integrase. Because integrase tended to aggregate, we immediately used it in assays after the purification. The obtained integrase was immediately injected into rabbits for immunization for the production of polyclonal anti-integrase. The molecular weight of the recombinant integrase was confirmed by Western blot analysis using the prepared antibody.

RNAi of Stat5a and Stat5b

The *Stat5a* RNAi (sc-37009; Santa Cruz Biotechnology) and the homologue *Stat5b* RNAi or control small-interfering RNA (siRNA) (sc-37007) were used according to the manufacturer's protocol (Santa Cruz Biotechnology). In a six-well tissue culture plate, 8.0×10^5 cells were seeded per well in a 2-ml antibiotic-free normal growth medium supplemented with fetal bovine serum. The lymphoma cells were incubated for 18 to 24 hours at 37°C in a CO_2 incubator. The siRNA duplex solution (solution A) was added directly to the diluted transfection reagent (solution B) using a pipette. The lymphoma cells were washed once with 2 ml of an siRNA transfection medium (sc-36868), and the medium was aspirated. We proceeded immediately to the next step. For each transfection, 0.8 ml of an siRNA transfection medium was added to each tube containing the siRNA transfection reagent mixture (solution A plus solution B). After gentle mixing, the mixture was overlaid onto the washed lymphoma cells, and the cells were incubated for 5 to 7 hours at 37°C in a CO_2 incubator. One milliliter of the normal growth medium containing twice the normal serum and antibiotic concentration (×2 normal growth medium) was added without removing the transfection mixture. Because of low viability, we removed the transfection mixture and replaced it with a ×1 normal growth medium. Next, the cells were incubated for an additional 96 hours. The medium was aspirated and replaced with fresh normal growth medium, and the protein was extracted and assayed by Western blotting using anti-STAT5A (ZYMED).

Preparation of Nuclear Extracts and Electromobility Shift Assay

The methods were previously described.[4] The probes were double-stranded oligonucleotides corresponding to the Stat-binding motif on the *bclxL* gene promoter (5′-GACTTTCCGAGGAAGGCATTTCGGAGAAGAC-3′). For a competition study, the extracts were incubated with 150 mol/L excess of the unlabeled probe.

Chromatin Immunoprecipitation Assay

The chromatin immunoprecipitation (ChIP) assay was performed as previously described.[14,16] The SL/Kh pre–B lymphoma clones were fixed with 1.0% formaldehyde at 4°C for 1 hour. Soluble chromatin was immunoprecipitated with 4 mg of primary antibodies overnight. The immune complex was eluted by incubation with a buffer containing 10 mmol/L DTT at 37°C for 30 minutes, diluted 50-fold, and reimmunoprecipitated with the second antibody. The same sets of fivefold serial dilutions of input DNA for determining the appropriate DNA concentration in the absence of nonspecific amplification and 2.5% to 5% purified ChIP DNA were subjected to PCR for 28 to 30 cycles. Control primers were used for determining the appropriate dilution.[14] After confirming that the nonspecific amplification was not observed by dilution, the immunoprecipitated DNA was amplified using the following primers: exon3 of *Stat5a*, 5′-CACGGCTGGCTCTCGATCCAC-3′; and, for the repeat region in 3′-LTR of *Emv11*, 5′-CAATAAAGCCTTTTGCTGTTGC-3′. To amplify the provirus 5′-LTR-*Stat5a* junctional DNA, the following primers were used: exon2 of *Stat5a*, 5′-CAAGAGCCGTCAGGAGCCGTC-3′; and, for the repeat region in 5′-LTR of *Emv11*, 5′-CAGATATCCTGTTTGGCCCTAG-3′. To amplify the provirus 5′-LTR (U3RU5), the following primers were used: 5′-TGAAAGACCCCTTCATAAGGCTTA (U3)-3′ and 5′-GGCTCCGTGGAAGAACTGAC-3′. To amplify the provirus 3′-LTR (U3RU5), the following primers were used: 5′-AGACAGGATTTCGGTAGTGCAGG (P15E)-3′ and 5′-ACAGCAAAGGCTTTATTGG-3′.

Statistical Analysis

Results are expressed as mean ± SD unless otherwise stated. All statistical analyses were performed using computer software (StatView; Abacus Concepts, Berkeley, CA). An unpaired *t*-test was used.

Results

MLV Integration Sites in the Stat5a *Gene*

In the current study, we analyzed a set of lymphoma clones with the *Emv11*-derived provirus integrated into the second intron of *Stat5a* (Figure 1A).[4] Integration sites were frequently found within a 46-bp palindromic sequence, including the most frequent site (ie, 1130). Southern hybridization using the MLV env probe or the *Stat5a* DNA probe demonstrated a newly acquired *MLV* genome integrating into *Stat5a* (Figure 1B, left and upper right).

There were significant differences in the expression level of STAT5A between the clones, whereas there were only minute differences in the integration sites; proviral genomes were identical. In particular, the expression of STAT5A was significantly higher in the lymphoma cells, with integration into sites between 1124 and 1134; in contrast, expression was not obvious in lymphoma cells with integration into other sites (Figure 1B, upper right, and Figure 1C). Thus, a minute difference between MLV integration sites led to large differences in the expression level of the target *Stat5a*. For the following analysis, we divided the clones into two groups on the basis of the expression level of STAT5A. Because constitutively and highly expressed STAT5A was observed in the clones with MLV integration into the 1124 to

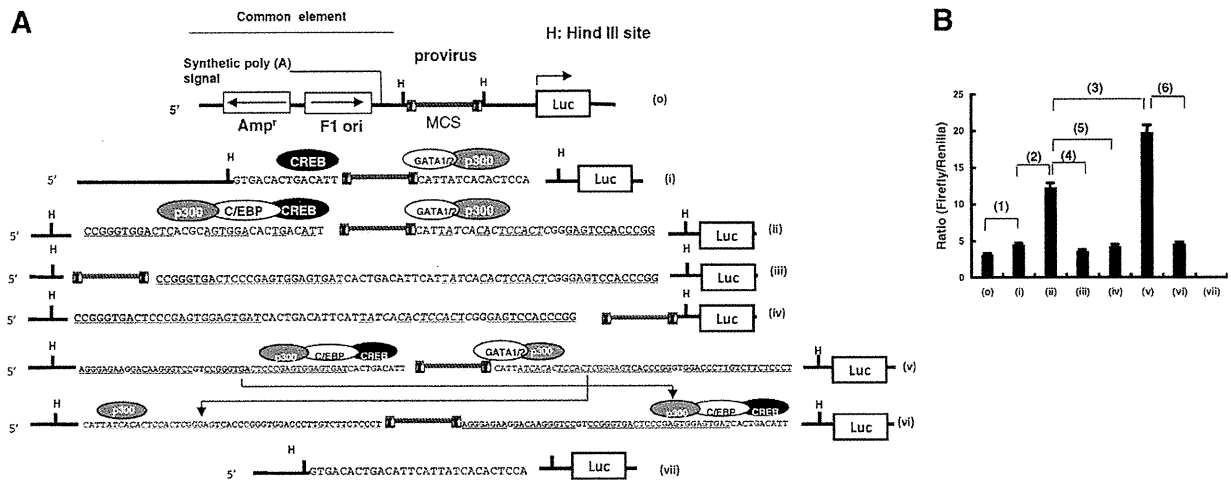

Figure 2. Luciferase assay using the Stat5a-derived sequence and *MLV* provirus genome. **A:** Sequences of the luciferase assay vectors. **o**, The pGL3-*Emv11* vector did not have the MLV flanking sequence. The pGL3 structure is shown. Luc represents Firefly luciferase in the pGL3 basic vector. The sequences of **i** through **vi** pGL3 vectors included the sequences flanking the proviral genome from the *Stat5a* sequence. MCS represents the location of the HindIII site (H) in the multiple-cloning site. **o**, **i**, **ii**, **iii**, **iv**, **v**, and **vi** in the schemes represent the ligated position of the provirus. The underlined letters indicate the palindromic motifs in the flanking sequences. The colored sequence is identical to the *Stat5a* sequence displayed in Figure 1A. The oligonucleotides CATT flanking the provirus were duplicated at the 5′ and 3′ ends of the provirus because such duplication in the integration site is commonly observed in *Emv11* integration sites. Red CATTATC at the 3′ end of the provirus is the GATA family binding sequence. Italicized *ATCACACTCCACTC* at the 3′ side flanking sequence is the p300 binding sequence. In the **iii**, **iv**, and **v** vectors, the proviral genome was flanked by identical sequences at different sites. **Arrows** in **v** and **vi** indicate the reverse of the flanking sequence in **v** for making the **vi** construct. Vector **vii** was the negative control vector, including the *Stat5a* sequence alone. **B:** Luciferase activity (ratio of Firefly to Renilla luciferase signal) in Ba/F3 cells containing vectors. Individual assays were independently performed five times. Individual columns represent the data obtained using the five vectors indicated. **o** through **v** represent the integration sites of the provirus ($n = 5$; 1, **o** versus **i**, $P = 0.031$; 2, **i** versus **ii**, $P = 0.024$; 3, **ii** versus **v**, $P = 0.011$; 4, **ii** versus **iii**, $P < 0.001$; 5, **ii** versus **iv**, $P < 0.001$; and 6, **v** versus **vi**, $P < 0.001$). Table 1 contains additional information. Luciferase activity values were evaluated using the Student's *t*-test.

1134 segment, they were named Stat5a^{high} clones. On the other hand, clones with integration into other sites were named Stat5a^{low} clones.

Furthermore, to evaluate how STAT5A expression was promoted by the integrated *MLV* genome, we attempted to analyze MLV-LTR-*Stat5a* chimera RNA. We found that the downstream *Stat5a* intron was serially transcribed after the RU5 element in the 5′-LTR of the provirus (Figure 1A). Therefore, the U3 segment of the 5′-LTR probably functioned as a promoter that up-regulated the expression of STAT5A.

Upstream and Downstream Sequences of the Provirus Influenced Reporter Gene Expression

The integration hot spots are within a 46-bp palindromic region containing transcription factor–binding sites. To examine whether the flanking sequence of the integration site might influence proviral promoter activity, luciferase assays were performed using seven pGL3-MLV-luciferase vectors consisting of a provirus or the downstream sequence, including CREB-, GATA-, and p300-binding motifs in *Stat5a* (Figure 2A). The Ba/F3 cells were selected for the assay because of their relative phenotypic similarity to the studied lymphoma cells, and luciferase reporter plasmids were transfected. Firefly luciferase activity was significantly up-regulated when the vector consisting of intact *Emv11*-derived proviral genome was flanked by the *Stat5a* sequence. In particular, activity was stronger when the *Emv11* proviral genome was flanked by a longer *Stat5a* sequence: 1, $P = 0.031$, o versus i; 2, $P = 0.024$, i versus ii; and 3, $P = 0.011$, ii versus v (Figure 2B). Of particular interest are vectors ii, iii, and iv, in which a proviral genome was integrated into different positions in the palindromic sequence, indicating that the symmetric location of the provirus in vector ii may be a critical factor for the higher activity of the promoter (4, $P < 0.001$, ii versus iii; and 5, $P < 0.001$, ii versus iv) (Table 1 and Figure 2B). In addition, the use of vector vi, which has the reverse flanking sequence of v, resulted in significant down-regulation of luciferase (6, $P < 0.001$, v versus vi) (Figure 2B), indicating that the flanking GATA- and p300-binding motifs also influence promoter activity.

Table 1. Results of the Dual Luciferase Assay Using Modified Emv11 Genomes

Vector	*Emv11*	*Emv11-5′Runx1-*	*Emv11-3′Runx1-*	*Emv11-5′LTR*	*Emv11-3′LTR*
i	0.008*	0.019*	0.021*	0.036*	0.214
ii	0.007*	0.028*	0.039*	0.018*	0.432
iii	0.071	0.267	0.398	0.291	0.291
iv	0.067	0.358	0.556	0.791	0.405
v	0.009*	0.032*	0.013*	0.012*	0.561

Data are given as *P* values for vector o versus five other vectors.
*Significant difference between vectors.

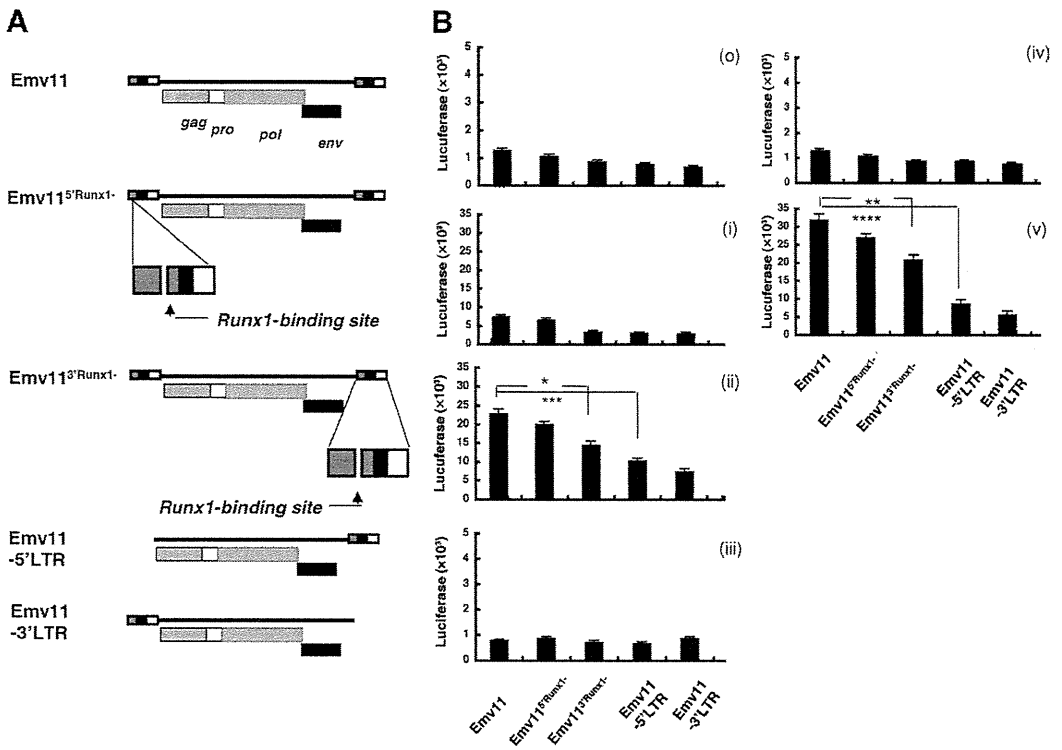

Figure 3. Luciferase assay using modified *Emv11* genomes. **A:** Structure of *Emv11* constructs in the luciferase assay vectors. Native *Emv11* is displayed at the top. Gag (group specific antigen), pro (protease), pol (polyprotein), and env (envelop protein) denote common retroviral genome elements. *Emv11*$^{5'Runx1-}$ and *Emv11*$^{3'Runx1-}$ represent *Emv11* lacking the *Runx1*-binding motif in 5′-LTR and 3′-LTR, respectively. *Emv11-5′-LTR* and *Emv11-3′-LTR* represent *Emv11* lacking 5′-LTR and *Emv11* lacking 3′-LTR, respectively. **B:** Luciferase assays. Luciferase activity (ratio of Firefly to Renilla luciferase signal) in Ba/F3 cells containing vectors. Individual assays were independently performed five times. Individual columns represent the data obtained using the five vectors indicated. **i** through **v** represent the vectors used. Table 2 contains additional information. For **ii**, $*P = 0.032$; $***P = 0.028$; **v**, $**P = 0.041$; $****P = 0.012$. Luciferase activity values were evaluated using the Student's *t*-test.

Activity of the Proviral Promoter Element

Next, we prepared five Firefly luciferase pGL3 vectors (o-v) at the HindIII site in the multicloning site into which defective proviral cDNA was inserted. These proviral DNAs in the vectors had defects in 3′-LTR (*Emv11*-3′-LTR), 5′-LTR (*Emv11*-5′-LTR), the Runx1-binding motif in 5′LTR (*Emv*$^{5'Runx1-}$), or the Runx1-binding motif in 3′-LTR (*Emv*$^{3'Runx1-}$) (Figure 3A). The vectors o through v carrying individual proviral cDNA were transfected into Ba/F3 pro–B cells.

The results showed that Firefly luciferase is significantly up-regulated even when the vector includes defective proviral genomes that are symmetrically flanked by palindromic motifs, as observed using intact *Emv11* vectors (Figure 3B and Table 1; $P < 0.05$ for i, ii, and v versus o). There were significant increases in luciferase activity when using *Emv11* inserted into ii and v instead of *Emv*$^{3'Runx1-}$ inserted into ii and v [Figure 3B ($*P = 0.032$ and $**P = 0.041$) and Table 2 ($n = 5$, ii and v)]. In addition, there were significant increases when using *Emv11* inserted into ii and v instead of *Emv11-5′LTR* (Figure 3B [$***P = 0.028$ and $****P = 0.012$] and Table 2 [$n = 5$, ii and v]). These data suggested that the Runx1-binding motif in 3′-LTR contributed to the up-regulation of downstream Firefly luciferase.

GATA2-Binding Motif in the Flanking Sequence

We analyzed the sequence motifs of the flanking sequences in host clone genomes. The GATA2-binding motif 5′-CAT-

Table 2. Results of the Dual Luciferase Assay

	Emv11 versus			
Vector	*Emv11-5′Runx1-*	*Emv11-3′Runx1-*	*Emv11-5′LTR*	*Emv11-3′LTR*
i	0.075	0.064	0.056	0.019*
ii	0.063	0.046*	0.028*	0.012*
iii	0.051	0.452	0.056	0.215
iv	0.085	0.673	0.081	0.366
v	0.062	0.037*	0.012*	0.006*

Data are given as *P* values for *Emv11*-carrying vectors versus individual defective *Emv11*-carrying vectors.
*Significant difference between vectors.

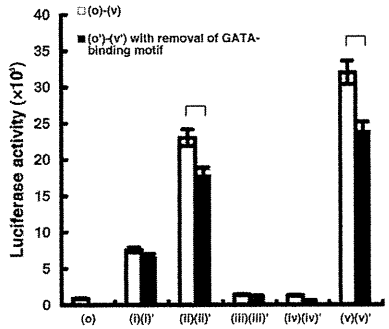

Figure 4. The GATA2-binding motif and retroviral promoter activity in luciferase assays. Relative luciferase activity is shown using vector constructs consisting of native or GATA2 motif defective flanking sequences. Individual assays were independently performed five times. The activity ratios (Firefly to Renilla luciferase) of **ii** and **v** were significantly higher than those of **ii**′ and **v**′, respectively (**ii** versus **ii**′, $^{*}P = 0.031$; **v** versus **v**′, $^{**}P = 0.028$). Measurements of luciferase activity were performed five times using individual vectors. Luciferase activity values were evaluated using the Student's *t*-test.

TATC-3′ was observed in integration site 1130 of the *Stat5a* sequence that was included in vectors i, ii, iii, iv, and v (Figure 2A). To evaluate the contribution of the motif to luciferase activity, assays were performed using five modified vectors (i′, ii′, iii′, iv′, and v′) from which the GATA2-binding motif in i, ii, iii, iv, and v, respectively, had been removed. The results revealed that luciferase activity was significantly higher when vectors ii and v were used relative to when vectors ii′ and v′, respectively, were used (Figure 4).

IP of Transcriptional Factor Binding to the Provirus-Stat5a Junction

We performed an IP assay using lymphoma clones and antibodies against proteins that have the potential to bind to LTR or the flanking sequences. The results revealed that Runx1 and integrase, GATA2 and integrase, GATA2 and p300, CREB-P1 and GATA2, and CREB-P1 and p300 form complexes (Figure 5A). Moreover, ChIP was performed using antibodies against Runx1, GATA2, and integrase. The precipitated DNA included *Emv11* 3′-LTR-*Stat5a* fusion genomic DNA in the Stat5a^{high} clones (Figure 5B). Moreover, reperformed IP of DNA fragments that were precipitated by an antibody against GATA2 or GATA1 was done using an antibody against Runx1 and p300. The results revealed that the *Emv11*-3′-LTR-*Stat5a* segment was coimmunoprecipitated with GATA2-Runx1

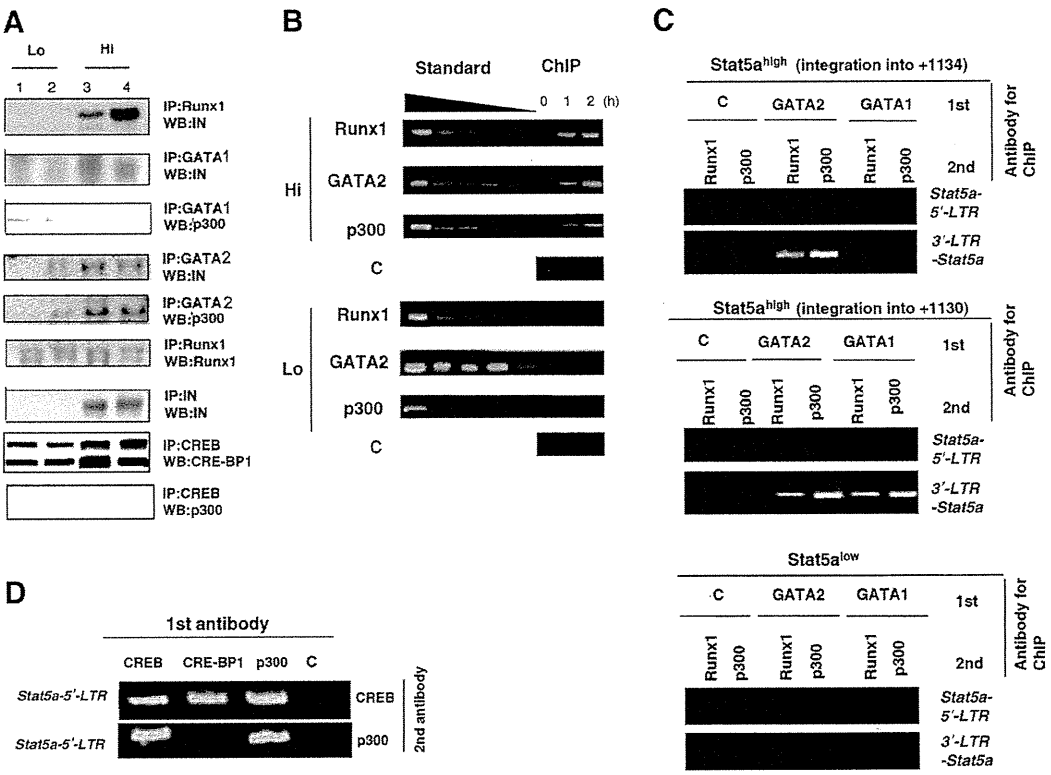

Figure 5. The IP of integrase (IN) complex and chromatin IP (ChIP) assays. Hi, Stat5a^{high} clones; Lo, Stat5a^{low} clones. **A:** The IP assay, lymphoma clone extracts. WB indicates Western blot. **Lanes 1** and **2:** Stat5a^{low} clones (integration sites, 1109 and 1115). **Lanes 3** and **4:** Stat5a^{high} clones (integration sites, 1126 and 1130). A photograph of WB using anti-CRE-BP1 revealed phosphorylated CRE-BP1 (upper band) and nonphosphorylated CRE-BP1. **B:** Reperformed ChIP-PCR assay. The chromatin preparation from 1.0×10^6 lymphoma cells was first immunoprecipitated with control and antibodies (first IP), and the immune complex was then eluted and reprecipitated with secondary antibodies (second IP). Primary and secondary antibodies used are shown. This also applies to the following figures. The upper photograph (*Stat5a-5′-LTR*) displays the results of PCR using primers between *Stat5a* and *Emv11* 5′-LTR. The lower photograph (*3′-LTR- Stat5a*) displays the results of PCR using primers between *Emv11* 3′-LTR and *Stat5a*. **C:** The ChIP-PCR assay. The photograph shows representative results of PCR using primers in the *Emv11* 3′-LTR and *Stat5a* third exon. The template DNA was extracted from chromatin preparations of 1.0×10^6 lymphoma cells and immunoprecipitated with antibodies against GATA2, Runx1, p300, or a normal rabbit IgG. Fivefold serial dilutions of total lymphoma DNA (standard) were amplified as an internal control of PCR using primers between −3346 and −2997 in the *Stat5a* gene (a and b, Stat5a^{high}; and c, Stat5a^{low}). **D:** Reperformed ChIP-PCR assay. The labels were identical to those in C.

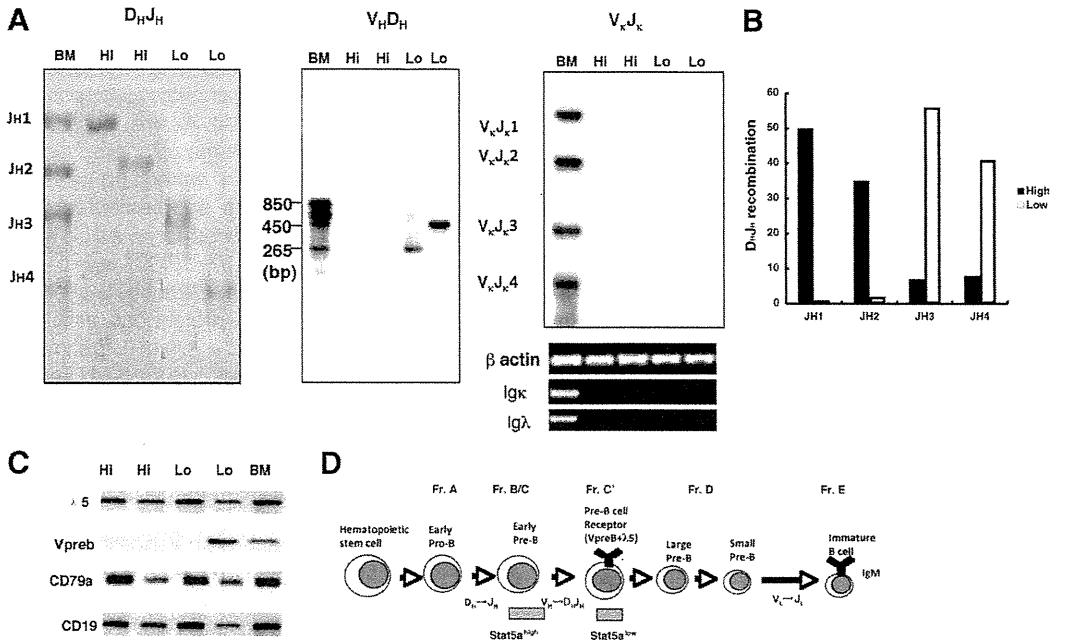

Figure 6. Development stages of pre–B lymphoma clones. **A:** Blots of D_HJ_H, IgH variable segment (V_H) and D_H, and VκDκ recombination. Hi indicates Stat5a^{high} clones; Lo, Stat5a^{low} clones; BM, pre–B cells of SL/Kh mice without the somatic *Emv11* integration 3 weeks after birth. **Lower:** Results of the RT-PCR assay for Igκ and Igλ expression. **B:** Type of D_HJ_H recombination in the clones. Percentages of the dominant type in individual Stat5a^{high} and Stat5a^{low} clones are presented. **C:** Results of RT-PCR for pre–B-cell receptor and other phenotypic markers. Hi indicates Stat5a^{high} clones (with integration into 1130); Lo, Stat5a^{low} clones (with integration into 1138); BM, pro–B cells obtained from SL/Kh mice 3 weeks after birth. **D:** Hardy's classification of Stat5a^{high} clones and Stat5a^{low} clones. Fr represents fraction. The stages of the B-cell lineage are shown.

and GATA2-p300 complexes in Stat5a^{high} clones (Figure 5C, a and b), whereas the *Emv11*-3′-LTR-*Stat5a* segment was not coimmunoprecipitated with these complexes (Figure 5C, c). In addition, the *Emv11*-3′-LTR-*Stat5a* segment from the clone with *Emv11* integration into 1130 was coimmunoprecipitated with GATA1-Runx1 and GATA1-p300 complexes (Figure 5C, b). Thus, the GATA-1 site could be referred to as a composite site that was formed *de novo* by the integration event. In addition, the *Stat5a-Emv11*-5′-LTR fusion segment was coimmunoprecipitated with the CRE-BP1-CREB and p300-CREB complexes (Figure 5D).

Integration Site Affects Maturation of Host Pro–B Lymphoma Cells

We investigated the integration site to determine its influence on the phenotype of host lymphoma clones. The STAT5A is involved in the malignant transformation of pro– and pre–B phenotypes.[17] The Stat5a^{high} clones completed IgH D_HJ_H recombination but not IgH variable segment–D_H recombination; on the other hand, Stat5a^{low} clones completed both D_HJ_H and IgH variable segment–D_H recombination. In both types of clones, Ig light chain recombination in Ig κ and Ig λ was not detected (Figure 6A). In the Stat5a^{high} clones, distal segments J_H1 and J_H2 were dominantly selected in D_HJ_H recombination, whereas in the Stat5a^{low} clones, proximal segments J_H3 and J_H4 were dominantly selected (significant findings) (Figure 6B). In addition, RT-PCR assays revealed that Stat5a^{high} clones were high for *λ5* but low for *Vpreb*, surrogate light chain components of pre–B-cell receptor; in contrast, Stat5a^{low} clones were constitutively high for both *λ5* and *Vpreb*. However, *Vpreb* expression was not constitutively high in Stat5a^{low} clones (Figure 6C). In summary, according to the murine B-cell classification of Hardy et al,[18] the Stat5a^{high} clones belonged to fraction B/C (pro– to early pre–B cells) and were more immature than other Stat5a^{low} clones that belonged to fraction C′ (pre–B cells) (Figure 6D). Thus, different integration sites of MLV influenced the development stage of the host cells.

Stimulation by IL-7 Receptor Suppressed Ig Light Chain Recombination in the Stat5a^{high} Lymphoma Clones

We then analyzed the effect of IL-7, one of the activation factors of signaling pathways that recruit STAT5A, on the development of Stat5a^{high} clones. The clones were first incubated for 24 hours in a medium without IL-7 to suppress intrinsic stimulation by IL-7 responses. Then, the knockdown of *Stat5a* was achieved by transfection of RNAi into the clones, performed with or without IL-7 for 120 hours. The knockdown was confirmed by Western blot analysis using an antibody toward STAT5A (Figure 7A).

After transfection, the expression of Ig κ and Ig λ was investigated by measuring the intensity of the Western blot. After incubation for 120 hours without *Stat5a* knockdown, IL-7 in the culture medium effectively suppressed Ig κ and Ig λ expression in Stat5a^{high} lymphoma clones (i versus ii); in contrast, the suppression was not evident in

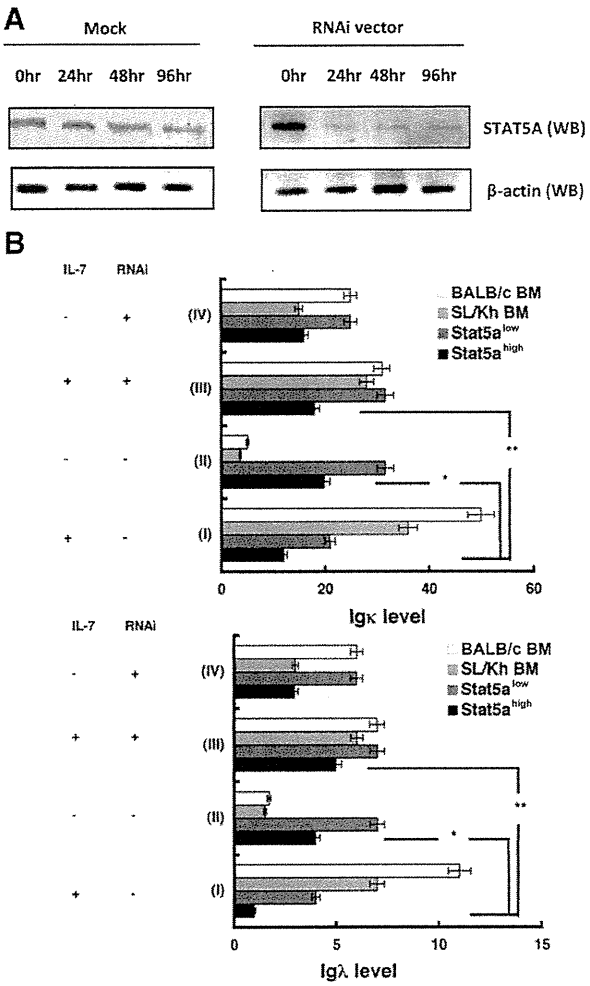

Figure 7. Arrest of Ig light chain (IgL) recombination in the Stat5a^{high} lymphoma clones supplemented with IL-7. **A:** Western blots (WBs) of the Stat5a^{high} clone with knockdown using control or both *Stat5a*- and *Stat5b*-RNAi with 50 ng/ml IL-7 or without IL-7 added. β-Actin was used as the control. **B:** The relative fluorescence intensity of Ig κ and Ig λ. For Stat5a^{high}, integration sites were 1124, 1126, 1130 (three clones), and 1134; Stat5a^{low}, integration sites were 1100, 1102, 1109, 1113, 1115, and 1138; SL/Kh BM, sorted normal pro–B cells without *Emv11* integration into *Stat5a* in the BM of SL/Kh mice; BALB/c BM, sorted control pro–B cells in the BM of BALB/c mice; + and −, presence and absence of 50 ng/ml IL-7 in the incubation medium for 96 hours, respectively. **Top: i** versus **ii**, $*P = 0.034$ ($n = 5$); and **i** versus **iii**, $**P = 0.041$ ($n = 5$). **Bottom: i** versus **ii**, $*P = 0.013$; and **i** versus **iii**, $**P = 0.023$. Assays were independently performed five times using four Stat5a^{high} clones and four Stat5a^{low} clones. Luciferase activity was assessed using Student's *t*-test.

Stat5a^{low} lymphoma clones (Figure 7). Incubation for 120 hours of the knockdown of *Stat5a* with IL-7 resulted in Ig κ and Ig λ expression in Stat5a^{high} lymphoma clones (i versus iii). Thus, the suppressive effect of IL-7 on Ig κ and Ig λ expression was exclusively evident in Stat5a^{high} lymphoma clones, indicating that the suppressive effect was dependent on the expression level of *Stat5a*.

IL-7 Receptor Stimulation Suppressed Apoptosis in the Stat5a^{high} Lymphoma Clones

There was an antiapoptotic effect of high expression of *Stat5a*. The clones were first incubated for 24 hours in a medium without IL-7 to suppress intrinsic stimulation by IL-7 responses. Next, supplying 50-ng/ml IL-7 during incubation resulted in significant up-regulation of the expression of Bcl-xL, an antiapoptotic protein, in the Stat5a^{high} clones (Figure 8A). As previously reported, the *bcl-xL* gene carries a gamma interferon activation site element in the promoter for enhancing dimeric STAT5A binding.[19] When IL-7 was supplemented, the relative densities of Bcl-xL and phosphorylated STAT5A closely correlated with each other ($P < 0.001$, $n = 5$) (Figure 8B).

Next, we performed an electromobility shift assay to investigate whether STAT5A protein can bind to the *bclxL* gene promoter after various levels of IL-7 stimulation using oligonucleotides corresponding to the STAT5A-binding motif on the murine *bcl-xL* gene promoter as a probe. After the addition of an antibody to the nuclear extracts, supershifts of the DNA binding complex were observed in an IL-7 dose-dependent manner (Figure 8C).

To confirm the effect of the increase in *bclxL* gene expression, the ratio of annexin V–positive apoptotic cells in the lymphoma clones was determined, with or without the addition of a cytokine supplement during the incubation. The results revealed that apoptotic cells were significantly less prevalent in Stat5a^{high} clones incubated with IL-7 (Figure 8D).

Discussion

The obtained data were used to construct a model to demonstrate why integration of a proviral genome into the specified location in the host sequence causes higher promoter activity and maturation arrest of the host cell (Figure 9). First, we found that Runx1, GATA2, and p300 bound to the 3′-LTR-*Stat5a* in the Stat5a^{high} clones (Figure 5, B and C). Next, we confirmed that CREB, CRE-BP1, and p300 bound to the 5′-LTR-*Stat5a* in the Stat5a^{high} clones (Figure 5D). This CREB protein has the potential to associate with CRE-BP1 and p300 in B cells and to control the transcription of the target gene. Therefore, CREB can be a scaffold for the recruitment of p300 on the LTR-*Stat5a* sequence DNA. Novel control of the CREB-dependent transcription of the target gene by a member of the regulator of G-protein signaling protein family in B cells has been reported.[20,21] The p300 increases target gene expression in several ways (ie, relaxing the chromatin structure at the gene promoter through its intrinsic histone-acetyltransferase activity and recruiting the general transcriptional machinery, including RNA polymerase II, to the promoter). In B cells, B-cell receptor linking induces histone lysine acetylation at the Bruton's tyrosine kinase promoter, correlating with marked recruitment of p300 to the locus.[22] Another recent study[23] reported that a paired box protein Pax5-mediated B-cell development was controlled by p300. Pax5 is a B-cell–specific activator protein that plays important roles in controlling the expression of lineage and differentiation stage–specific genes during B lymphopoiesis. Furthermore, p300 is a coactivator for transcription factor REL and is C terminally truncated in the human diffuse large B-cell lymphoma cell line.[24] Thus, p300 contributes to B-

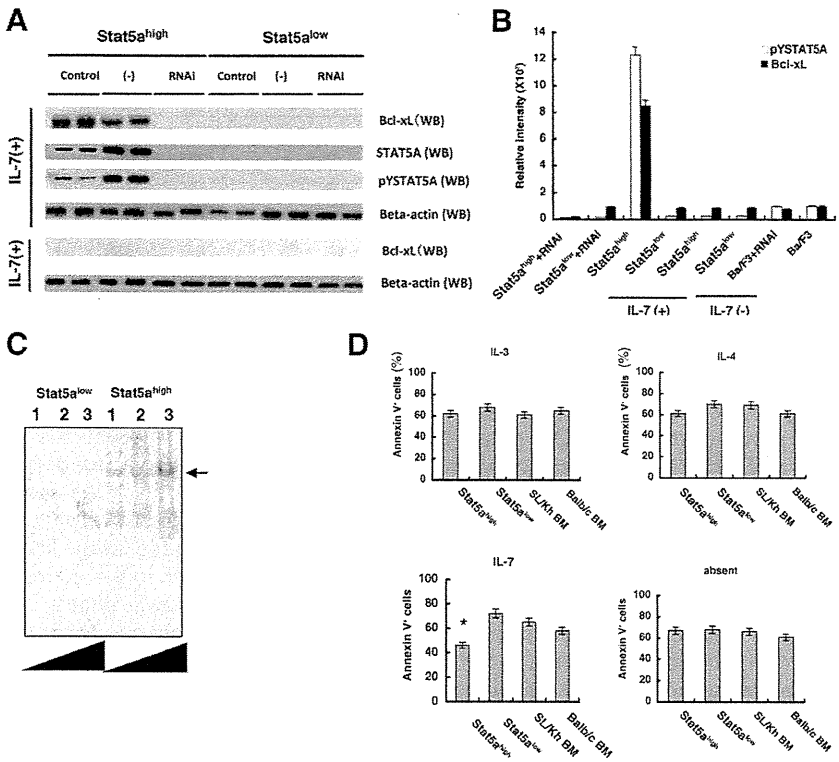

Figure 8. Expression of Bcl-xL in lymphoma clones. **A:** The RT-PCR assay of *bcl-xL* using Stat5a^{high} and Stat5a^{low} lymphoma clones. WB indicates Western blot. **B:** Relative density of the WBs for phosphorylated STAT5A (pYSTAT5A) and Bcl-xL. The density was measured with chemiluminator LumiVision. **C:** Identification of Stat5A binding by supershift analysis. **Lanes 1**, **2**, and **3:** Nuclear extracts of lymphoma cells stimulated with 0, 20, and 40 ng/mL of recombinant murine IL-7, respectively. The **arrow** highlights the supershift. **D:** Percentage of annexin V–positive cells in the population of lymphoma cells incubated with or without cytokines ($n = 5$, $^*P < 0.05$, Stat5a^{high} versus others).

cell development and lymphomagenesis. The histone-acetyltransferase activity of p300 modulates human T-lymphotropic virus-I LTR transcriptional activity.[25] Herein, we hypothesize that p300 bindings may promote the expression of MLV and the target *Stat5a*. Although there have been few reports regarding the relation of p300 with MLV LTR transcriptional activity, we suppose that direct p300 binding to the upstream sequence of the provirus or an indirect effect via association with CREB binding to the upstream sequence up-regulates the transcriptional activity; in addition, p300 binding to the downstream sequence may contribute to the transcriptional activity

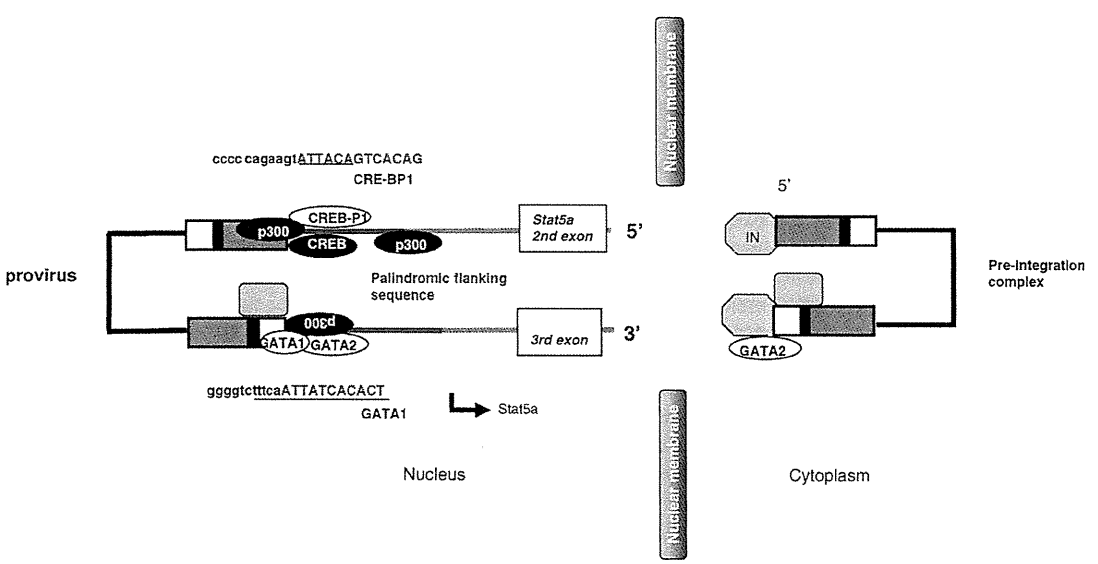

Figure 9. Model of the complex promoting transcription of the target gene. Transcription factor complexes on the LTR-*Stat5a* sequence. The provirus is integrated into 1130 and into another site. Transcription of LTR started from the RU5 element on the proviral genome. Lines by the sequence represent the CRE-BP1 and GATA1 motifs. The sequences next to the viral *Stat5a* segment display the motifs of p300, CREB, CRE-BP1, GATA2, Runx1, and GATA1. Lowercased letters represent MLV-LTR element sequences; and uppercased letters, *Stat5a* sequences. IN indicates integrase.

Table 3. MLV Integrations Near the Coding Region

Host gene located downstream of the integration site	Mouse chromosome		
	Size, bp	No.	Location
ATPase, H^+-transporting, V1 subunit G isoform 2	3,623 and 3,723	17	NT_039649
Fc-γ receptor	155,834	3	NT_39240
GRP1-binding protein GRSP1 (Frmd4b)	16,330	6	NT_039353.7
Myosin, heavy polypeptide 9, nonmuscle isoform 1	22,229	15	NT_039621.7
Similar to Gpd1l protein	5,189	5	NW_001030784.1
Similar to high-mobility group box 1	22,452	15	NT_039621.7
3-Hydroxyanthranilate-3,4-dioxygenase	292,004	17	NW_001030622.1
Testicular serine protease 1	7,060	1	NT_039170.7

downstream of *Stat5a* (Figure 2A, ii). This multiplier effect of p300 downstream and upstream of the provirus may contribute to a significant increase in the proviral promoter activity and the higher expression of *Stat5a*. A plausible regulation is that the palindromic sequence contributed to the stabilization of the relaxed chromatin by generation of a secondary structure, such as a cruciform or hairpin structure in the single-stranded DNA. Significantly, acetylation of HIV-1 integrase by p300 regulates viral integration.[26,27] Studamire and Goff[28] reported host proteins interacting with the Moloney murine leukemia virus integrase. In the future, other interacting proteins will be identified, and p300 may be among them.

When MLV is integrated into the most frequent integration site (ie, 1130), the *de novo* GATA1-binding motif appears in the provirus-host junctional sequence (Figure 5C). Indeed, the IP assay shown in Figure 5C indicates that GATA1 binds to the *Emv11* 3′-LTR-*Stat5a* segment. Thus, the proviral terminal sequence DNA connected to the host sequence DNA carries several potential transcription factor–binding motifs. The binding GATA1 may be controlled by acetylation by CRE-BP1.[29]

In the current study, a significant amount of integrase was unexpectedly observed in the lymphoma clones. The mean ± SD of 68 ± 17 nonclonal integration sites was identified in an examined clone by an inverse PCR method; the integration sites that are relatively close to the coding regions are listed in Table 3. These data suggested that MLV integration constitutively occurred in the lymphoma cells. In actuality, expression of ecotropic virus *Emv11* by neonatal injection of maternal resistance factor inhibits lymphomagenesis.[11] It is probable that MLV particles were provided by individual lymphoma cells and that the MLV reinfected neighboring lymphoma cells during tumor development, with translocation of integrase into the nucleus. This SL/Kh strain of mice possesses more than six copies of endogenous retroviruses in the germ line (Figure 1B). Six is a far higher number than that in other strains of mice, such as AKR.[12] A previous report[11] shows that two of these endogenous retroviruses have the potential to be transcribed into producing complete viral particles. In this study, we found three endogenous retroviruses other than *Emv11* (see Supplemental Table S1 at *http://ajp.amjpathol.org*). These endogenous retroviral transcriptional mechanisms and functions are not entirely understood, and further study will be required for consideration of a model in which integrase interacts with transcriptional factors in the host cells. Notably, Kitamura et al reported that human endogenous retrovirus K10 encodes a functional integrase.[30]

Our data clearly show that the *Emv11* integration site influences host phenotype via the maturation arrest of the *IgH* recombination. These influences by the integration site remain poorly understood, and insufficient attention has been paid to host phenotypic changes aside from *Emv11* tumorigenesis. However, as shown in the current study, the integration site can have variable effects on host phenotype via integration. Although our study is limited to *IgH* recombination in the presence of IL-7, the cell culture conditions may affect the host cell phenotype by the integration. In this model, we added evidence that STAT5A may contribute to the tumorigenesis of pre–B lymphoma/leukemia. In actuality, there have been reports[31,32] that mutations of Janus kinase 2, which phosphorylates STAT5, in acute lymphocytic leukemia are associated with Down's syndrome. Thus, the contribution of STAT5 to leukemogenesis has been commonly accepted. Our study model could be one of the models of lymphoblastic tumorigenesis.

The MLV vectors are essential tools for the generation of induced pluripotent stem cells. Nevertheless, the data presented herein provide significant information about the phenotypes of transgenic animals carrying the MLV vector. A minute difference between MLV integration sites can lead to large differences in host phenotype, suggesting that caution should be advised in monitoring integration sites when working with MLV vectors.

Acknowledgments

We thank Dr. Hiroshi Hiai (Kyoto University, Kyoto, Japan) for overview and critical advice regarding the manuscript; Dr Tasuku Honjo, Kyoto University, for critical advice regarding the manuscript; and Ms. H. Saito for providing technical assistance.

References

1. Hacein-Bey-Abina S, Von Kalle C, Schmidt M, McCormack MP, Wulffraat N, Leboulch P, Lim A, Osborne CS, Pawliuk R, Morillon E, Sorensen R, Forster A, Fraser P, Cohen JI, de Saint Basile G, Alexander I, Wintergerst U, Frebourg T, Aurias A, Stoppa-Lyonnet D, Romana S, Radford-Weiss I, Gross F, Valensi F, Delabesse E, Macintyre E, Sigaux F, Soulier J, Leiva LE, Wissler M, Prinz C, Rabbitts TH, LE Deist F, Fischer A, Cavazzana-Calvo M: LMO2-associated clonal

T cell proliferation in two patients after gene therapy for SCID-X1. Science 2003, 302:415–419
2. Nakagawa M, Koyanagi M, Tanabe K, Takahashi K, Ichisaka T, Aoi T, Okita K, Mochiduki Y, Takizawa N, Yamanaka S: Generation of induced pluripotent stem cells without Myc from mouse and human fibroblasts. Nature Biotechnol 2008, 26:101–106
3. Akagi K, Suzuki T, Stephens RM, Jenkins NA, Copeland NG: RTCGD: retroviral tagged cancer gene database. Nucleic Acids Res 2004, 32:D523–D527
4. Tsuruyama T, Nakamura T, Jin G, Ozeki M, Yamada Y, Hiai H: Constitutive activation of Stat5a by retrovirus integration in early pre-B lymphomas of SL/Kh strain mice. Proc Natl Acad Sci U S A 2002, 99:8253–8258
5. Matsumura I, Kitamura T, Wakao H, Tanaka H, Hashimoto K, Albanese C, Downward J, Pestell RG, Kanakura Y: Transcriptional regulation of the cyclin D1 promoter by STAT5: its involvement in cytokine-dependent growth of hematopoietic cells. EMBO J 1999, 18:1367–1377
6. Nosaka T, Kawashima T, Misawa K, Ikuta K, Mui AL, Kitamura T: STAT5 as a molecular regulator of proliferation differentiation and apoptosis in hematopoietic cells. EMBO J 1999, 17:4754–4765
7. Kirito K, Watanabe T, Sawada K, Endo H, Ozawa K, Komatsu N: Thrombopoietin regulates Bcl-xL gene expression through Stat5 and phosphatidylinositol 3-kinase activation pathways. J Biol Chem 2002, 277:8329–8337
8. Chowdhury D, Sen R: Stepwise activation of the immunoglobulin mu heavy chain gene locus. EMBO J 2000, 20:6394–6403
9. Sexl V, Piekorz R, Moriggl R, Rohrer J, Brown MP, Bunting KD, Rothammer K, Roussel MF, Ihle JN: Stat5a/b contribute to interleukin 7-induced B-cell precursor expansion but abl- and bcr/abl-induced transformation are independent of Stat5. Blood 2000, 96:2277–2283
10. Schwaller J, Parganas E, Wang D, Cain D, Aster JC, Williams IR, Lee CK, Gerthner R, Kitamura T, Frantsve J, Anastasiadou E, Loh ML, Levy DE, Ihle JN, Gilliland DG: Stat5 is essential for the myelo- and lymphoproliferative disease induced by TEL/JAK2. Mol Cell 2000, 6:693–704
11. Abujiang P, Yamada Y, Haller O, Kobayashi H, Kamoto T, Lu LM, Ogawa M, Ishimoto A, Katoh H, Kanehira K, Ikegami S, Fukumoto M, Hiai H: The origin of SL family mice. Lab Anim Sci 1996, 62:410–417
12. Mucenski ML, Bedigian HG, Shull MM, Copeland NG, Jenkins NA: Comparative molecular genetic analysis of lymphomas from six inbred mouse strains. J Virol 1988, 62:839–884
13. Pennycook JLMH, Marshall AJ, Wu GE: PCR assays for endogenous Ig gene rearrangement. Immunology Methods Manual, vol 1. Edited by I Lefkovits. San Diego, Academic Press, 1997, pp 564
14. Ye SK, Maki K, Kitamura T, Sunaga S, Akashi K, Domen J, Weissman IL, Honjo T, Ikuta K: Induction of germline transcription in the TCRγ locus by Stat5: implications for accessibility control by the IL-7 receptor. Immunity 1999, 11:213–223
15. Ishihara K, Satoh I, Nittoh T, Kanaya T, Okazaki H, Suzuki T, Koyama T, Sakamoto T, Ide T, Ohuchi K: Preparation of recombinant rat interleukin-5 by baculovirus expression system and analysis of its biological activities. Biochim Biophys Acta 1999, 1451:48–58
16. Shang Y, Hu X, DiRenzo J, Lazar MA, Brown M: Cofactor dynamics and sufficiency in estrogen receptor-regulated transcription. Cell 2000, 103:843–852
17. Santos SC, Lacronique V, Bouchaert I, Monni R, Bernard O, Gisselbrecht S, Gouilleux F: Constitutively active STAT5 variants induce growth and survival of hematopoietic cells through a PI 3-kinase/Akt dependent pathway. Oncogene 2001, 20:2080–2090
18. Hardy RR, Carmack CE, Shinton SA, Kemp JD, Hayakawa K: Resolution and characterization of pro-B and pre-pro-B cell stages in normal mouse bone marrow. J Exp Med 1991, 173:1213–1225
19. Socolovsky M, Fallon A, Wang S, Brugnara C, Lodish H: Fetal anemia and apoptosis of red cell progenitors in Stat5a-/-5b-/- mice: a direct role for Stat5 in Bcl-xL induction. Cell 1999, 98:181–191
20. Vo N, Goodman RH: CREB-binding protein and p300 in transcriptional regulation. J Biol Chem 2001, 276:13505–13508
21. Xie Z, Geiger TR, Johnson EN, Nyborg JK, Druey KM: RGS13 acts as a nuclear repressor of CREB. Mol Cell 2008, 31:660–670
22. Spiegelman BM, Heinrich R: Biological control through regulated transcriptional coactivators. Cell 2004, 119:157–167
23. Lee IS, Choi WH, Kim JY, Jeong JY, Kim MJ, Nam JH, Kim JH, Seo SB, Pak JH: Transcriptional regulation of the murine 1-cys peroxiredoxin gene by the B cell-specific activator protein, Pax5. J Cell Biochem 2008, 104:465–476
24. Garbati MR, Alço G, Gilmore TD: Histone acetyltransferase p300 is a coactivator for transcription factor REL and is C-terminally truncated in the human diffuse large B-cell lymphoma cell line RC-K8. Cancer Lett 2010, 291:237–245
25. Michael B, Nair AM, Datta A, Hiraragi H, Ratner L, Lairmore MD: Histone acetyltransferase (HAT) activity of p300 modulates human T lymphotropic virus type 1 p30II-mediated repression of LTR transcriptional activity. Virology 2006, 354:225–239
26. Cereseto A, Manganaro L, Gutierrez MI, Terreni M, Fittipaldi A, Lusic M, Marcello A, Giacca M: Acetylation of HIV-1 integrase by p300 regulates viral integration. EMBO J 2005, 24:3070–3081
27. Raghavendra NK, Shkriabai N, Graham RLJ, Hess S, Kvaratskhelia M, Wu L: Identification of host proteins associated with HIV-1 preintegration complexes isolated from infected CD4+ cells. Retrovirology 2010, 7:66
28. Studamire B, Goff SP: Host proteins interacting with the Moloney murine leukemia virus integrase: multiple transcriptional regulators and chromatin binding factors. Retrovirology 2008, 5:48
29. Hung HL, Lau J, Kim AY, Weiss MJ, Blobel GA: CREB binding protein acetylates hematopoietic transcription factor GATA-1 at functionally important sites. Mol Cell Biol 1999, 19:3496–3505
30. Kitamura Y, Ayakawa T, Ishikawa T, Kanda T, Yoshiike K: Human endogenous retrovirus K10 encodes a functional integrase. J Virol 1996, 70:3302–3306
31. Bercovich D, Ganmore I, Scott LM, Wainreb G, Birger Y, Elimelech A, Shochat C, Cazzaniga G, Biondi A, Basso G, Cario G, Schrappe M, Stanulla M, Strehl S, Haas OA, Mann G, Binder V, Borkhardt A, Kempski H, Trka J, Bielorei B, Avigad S, Stark B, Smith O, Dastugue N, Bourquin JP, Tal NB, Green AR, Izraeli S: Mutations of JAK2 in acute lymphoblastic leukaemias associated with Down's syndrome. Lancet 2008, 372:1484–1492
32. Kearney L, Gonzalez De Castro D, Yeung J, Procter J, Horsley SW, Eguchi-Ishimae M, Bateman CM, Anderson K, Chaplin T, Young BD, Harrison CJ, Kempski H, So CW, Ford AM, Greaves M: Specific JAK2 mutation (JAK2R683) and multiple gene deletions in Down syndrome acute lymphoblastic leukemia. Blood 2009, 113:646–648